FEDERAL UNIVERSITY OF OURO PRETO (UFOP)

SCHOOL OF PHARMACY

PHARMACY DEPARTMENT

PLASMONIC SILVER NANOPARTICLES: *IN-SITU* MONITORING AND EVALUATION OF CYTOTOXICITY

JÚLIA SANTOS AVELAR

OURO PRETO-MG

2021

JÚLIA SANTOS AVELAR

PLASMONIC SILVER NANOPARTICLES: *IN-SITU* MONITORING AND EVALUATION OF CYTOTOXICITY

Bachelor thesis presented to the Examining Evaluators of the Federal University of Ouro Preto as a requirement for obtaining the degree of Bachelor of Pharmacy. Advisors: Prof. Huayna Terraschke (Christian Albrechts University, Germany) and Prof. Vanessa C. F. Mosqueira (Federal University of Ouro Preto, Brazil). Co-advisor: MSc. Maria Alice de Oliveira

OURO PRETO-MG

2021

SISBIN - SISTEMA DE BIBLIOTECAS E INFORMAÇÃO

A948p Avelar, Julia Santos .
Plasmonic silver nanoparticles [manuscrito]: in-situ monitoring and evaluation of cytotoxicity. / Julia Santos Avelar. - 2021.
66 f.

Orientadora: Profa. Dra. Vanessa Carla Furtado Mosqueira.
Coorientadora: Ma. Maria Alice Oliveira.
Monografia (Bacharelado). Universidade Federal de Ouro Preto. Escola de Farmácia. Graduação em Farmácia .

1. Nanoparticulas . 2. Reatores químicos. 3. Radiação sincrotrônica. 4. Citotoxicidade. 5. Macrófagos. I. Mosqueira, Vanessa Carla Furtado. II. Oliveira, Maria Alice. III. Universidade Federal de Ouro Preto. IV. Título.

CDU 620.3

Bibliotecário(a) Responsável: Soraya Fernanda Ferreira e Souza - SIAPE: 1.763.787

ATA DA SESSÃO DE DEFESA DA 524ª MONOGRAFIA DO CURSO DE FARMÁCIA DA ESCOLA DE FARMÁCIA DA UNIVERSIDADE FEDERAL DE OURO PRETO. Aos 23 dias do mês de setembro de 2021, quinta-feira, realizou-se, a partir das 08 horas, por videoconferência, a sessão de defesa de monografia do candidato ao grau de Farmacêutico Generalista, **Júlia Santos Avelar, matrícula 15.1.2140,** intitulada **"Plasmonic silver nanoparticles: *in-situ* monitoring and evaluation of cytotoxicity".** A banca examinadora foi constituída pela Profa. Dra. Raquel Silva Araújo (UFOP), pelo Dr. Leonardo César de Moraes Teixeira (UFMG), pela orientadora Profa. Dra. Huayna Terraschke (Christian Albrechts University - Germany) e pela orientadora Profa. Dra. Vanessa Carla Furtado Mosqueira (DEFAR-UFOP). O trabalho foi co-orientado pela doutoranda Maria Alice de Oliveira. De acordo com o regulamento do curso, o orientador, presidente da banca, abriu a sessão, passando a palavra ao candidato, que fez a exposição do seu trabalho. Em seguida, foi realizada a arguição pelos examinadores na ordem registrada acima, com a respectiva defesa do candidato. Finda a arguição, a Banca Examinadora se reuniu, sem a presença do candidato e do público, tendo deliberado pela sua **APROVAÇÃO**, com a NOTA **9,5**. Comunicou-se ao candidato que essa nota somente será liberada para a PROGRAD, após a entrega do exemplar definitivo de acordo com as normas estabelecidas pelo Sistema de Bibliotecas e Informação (Sisbin), com as devidas correções sugeridas pela banca e com o aval escrito do orientador. Nada mais havendo para constar, a presente ata foi lavrada e após a leitura pública seguirá assinada pelo orientador e pelo presidente do Colegiado. Ouro Preto, 23 de setembro de 2021.

Profa. Dra. Vanessa Carla Furtado Mosqueira
(Orientador)

Profa. Dra. Nancy Scardua Binda
(Presidente do Colegiado de Farmácia)

ACKNOWLEDGMENTS

First of all, I would like to thank my family, especially my parents, for allowing me to be where I am today and for always doing everything, possible to the impossible, so that I could achieve my dreams. Thank you, you are my basis.

To my friends, especially the Family - República Pecado Original and the T* (group that should not be named), for always encouraging me and showing me that I am capable. I am very happy to share life with each one of you!

To Professor Huayna Terraschke for giving me the best opportunity/experience of my life and opening my eyes to the greatness of science, words would not be enough to describe my gratitude, thank you very much for all your teachings. To 'Die Lumis' for being my family during my time in Germany, especially, Jonas (thank you for your daily patience), Laura, Jasper, Ban and Patrick.

To Professor Vanessa Mosqueira for helping me from the beginning and stimulating me to always do my best, thank you for adding immensely to this work. To the LDG Nano group for the welcome, especially Maria Alice and Carlos for all the teachings and care, even if for a short time of work. Without you, none of this would be possible.

Finally, the Federal University of Ouro Preto for providing me a free and quality study, thank you!

ABSTRACT

For some years, the interest in the synthesis of plasmonic silver nanoparticles (Ag NPs) has grown considerably, in view of their numerous applications, such as tumor biomarkers and drug carriers. However, for the effectiveness of the application of Ag NPs an adequate control of the synthesis and consequently of the structural as well as optical properties of Ag NPs is necessary. This work aims to highlight synthesis and characterization methodologies that allow a more effective control of the formation of Ag NPs, using a flow and batch reactor. For this purpose, *in-situ* and *ex-situ* measurements of pH value, optical spectroscopy, synchrotron-based X-ray diffraction and dynamic light scattering have been performed in Germany. After storage the Ag NPs were characterized again in respect of their size and zeta potential. In an attempt to avoid aggregation of the Ag NPs and increase their stability, a non-ionic surfactant, the Polyoxyethylene-polyoxypropylene Block Copolymer (Pluronic® F68) was added to the surface of Ag nanoparticles. Due to the potential pharmaceutical applications of Ag NPs, their cytotoxicity was investigated. It is noteworthy that Ag NPs cytotoxicity toward RAW 264.7 macrophage cell line was dose-dependent for the sample with lower size and also size-dependent in our experimental conditions.

Key Words: Plasmonic nanoparticles; silver nanoparticles; flow reactor; synchrotron radiation; cytotoxicity; macrophage.

RESUMO

O interesse na síntese de nanopartículas plasmônicas, especificamente as de prata, cresceu consideravelmente ao longo dos últimos anos, tendo em vista as suas inúmeras aplicações, tais como, biomarcadores tumorais e carreadores de fármaco. Contudo, para a eficácia da aplicação das Ag NPs é necessário um controle adequado da síntese e das propriedades estruturais e ópticas das Ag NPs. A partir disto, este trabalho visa destacar metodologias de síntese e caracterização que permitam um controle mais eficaz da formação de Ag NPs, utilizando reatores de fluxo e em batelada. Para este fim, foram realizadas, na Alemanha, análises *in-situ* e *ex-situ* do valor de pH, espectroscopia óptica, difração de raios X baseada em radiação sìncrotron e dispersão dinâmica da luz. Após armazenamento, as Ag NPs foram novamente caracterizadas no que diz respeito ao seu tamanho de partícula e potencial zeta. Numa tentativa de evitar a agregação das Ag NPs e aumentar a sua estabilidade, um tensioativo não-iônico, o triblock polyethylene oxide-block-polypropylene oxide-block-polyethylenoxide (Pluronic® F68) foi adicionado à superfície das nanopartículas de prata. Devido as potenciais aplicações farmacêuticas das Ag NPs, a sua citotoxicidade foi investigada. É de salientar que a citotoxicidade das Ag NPs para a linhagem celular de macrófagos RAW246 é dose-dependente para as amostras que apresentaram menor tamanho de partícula e também tamanho-dependente nas nossas condições experimentais.

Palavras-chave: Nanopartículas plasmônicas; nanopartículas de prata; reator de fluxo; radiação sincrotron; citotoxicidade; macrófago.

FIGURE LIST

Figure 1: Schematic of plasmon oscillation in spherical plasmonic nanoparticle showing the displacement of the conduction electron charge cloud relative to the nuclei. 11
Figure 2: Application of metal nanoparticles (MNPs) in various fields. 14
Figure 3: The Lycurgus cup. Gold and silver NPs in the glass resulted in incredible and unique color effects. 15
Figure 4: Schematic representation of the protocol of the Turkevich's method applied for the synthesis of plasmonic NPs, using gold as example. 18
Figure 5: Stabilizing silver nanoparticles (Ag NPs) by steric repulsive forces. 19
Figure 6: Schematic representation of the synthesis of SNPs with water-in-oil (w/o) microemulsion 20
Figure 7: Photograph of (a) Violet (b) Blue (c) Purple (d) Green (e) Yellow (f) Orange and (g) Red Ag NPs suspensions 22
Figure 8: Absorption spectra of different colors of silver nanoparticles suspensions (a) Violet (b) Blue (c) Purple (d) Green (e) Yellow (f) Orange (g) Red. 22
Figure 9: Cytotoxic effect of drug conjugated silver nanoparticles. 24
Figure 10: Setup applied for the experiments using the flow reactor. Metrohm dosing system used can be seen on the right side. 31
Figure 11: Setup for experiment conducted in batch regime at the beamline P23 at DESY 32
Figure 12: Schematic representation of the Pluronic® F68 addition in the selected samples from nine experiments of synthesis of Ag NPs 38
Figure 13: Experiment I using the flow reactor, enabling visualization with the naked eye of the yellow coloration throughout the reaction (A) and the solution after the synthesis (B) 41
Figure 14: Picture of the solution after the synthesis of Ag NPs from the experiment II. 42
Figure 15: Representation of the flow reactor during experiment III, showing the difference in coloration of the Ag NPs formed during the reaction. 42
Figure 16: Comparison of the *ex-situ* XRD measurements for experiment III (black curve) with the calculated powder diffraction for silver (red curve). 43

Figure 17: Ag NPs suspension after the NPs synthesis on the experiment IV. 44
Figure 18: Comparison of the ex-situ XRD values for product of experiment IV. The black curve represents the measured values and for the red curve the ones for the Ag calculated diffraction partners. 45
Figure 19: Experiment V using the flow reactor, enabling visualization with the naked eye of the yellow coloration throughout the reaction time.....46
Figure 20: Comparison of the ex-situ XRD values for product of experiment V. The red curve represents the measured values and for the black curve the ones for the Ag calculated diffraction partners. 46
Figure 21: The product suspension after the synthesis of Ag NPs from the experiment VI 47
Figure 22: Particle size distribution for product suspension of experiment VII.....48
Figure 23: Suspension after the synthesis of Ag NPs from the experiment VIII.....49
Figure 24: Particle size distribution of product of experiment VIII 49
Figure 25: 2D *(A)* and 3D *(B)* plot of absorbance measurements for experiment IX.The experiment was performed on the Beamline P02.1 at DESY, Hamburg. 50
Figure 26: Graph of absorbance measurements for experiment IX, comparing reaction time X absorption. 51
Figure 27: Comparison between the synthesized in-situ X-ray diffraction partners (black curve) and the simulated values for silver (red curve). 52
Figure 28: Comparison between the ex-situ X-ray diffraction patterns for the synthesized (black curve) and the simulated ones for silver (red curve). 53
Figure 29: Comparison between temporal evolution of XRD analysis, absorption and pH measurements during the Ag NPs synthesis. 54
Figure 30: Cell viability of RAW 264.7 cells after treatment with Ag NPs for 24h 58

TABLE LIST

Table 1: Standard Potential of silver and examples of commonly used reducing agents in the synthesis of silver nanoparticles. 16

Table 2: Cell line, particle size, concentration and IC50 for Ag NPs reported on literature 26

Table 3: Concentrations of the reagents used to synthesize Ag NPs in the 9 experiments. 33

Table 4: Quantification of silver present in experiments II and VIII……. 39

Table 5: Zeta potential values for the Ag NPs synthesized and for the Ag NPs with Pluronic® F68, at T0 (time zero) and at T21 (after 21 days from the first analysis). 55

Table 6: Particle size distribution (PSD) values for the Ag NPs synthesized and for the Ag NPs with Pluronic® F68, at T0 (time zero) and at T21 (after 21 days from the first analysis) 56

ABBREVIATIONS LIST

Ag	*Silver*
Ag NPs	*Silver nanoparticles*
$AgNO_3$	*Silver nitrate*
Au	*Gold*
Au NPs	*Gold nanoparticles*
CAU	*Christian Albrechts University*
DESY	*Deutsches Elektronen-Synchrotron*
DLS	*Dynamic light scattering*
FTIR	*Fourier transform infrared spectroscopy*
MNPs	*Metal nanoparticles*
$Na_3C_6H_5O_7$	*Trisodium citrate*
$N_2H_6SO_4$	*Hydrazine sulphate*
NPs	*Nanoparticles*
PDI	*Polydispersity index*
PSD	*Particle size distribution*
SEM	*Scanning electron microscopy*
SPR	Surface plasmon resonance
TEM	*Transmission electron microscopy*
UFOP	*Federal University of Ouro Preto*
XRD	*X-Ray Diffraction*

SUMMARY

1. INTRODUCTION 11
2. LITERATURE REVIEW 14
2.1 Plasmonic Nanoparticles 14
2.2 Synthesis of Plasmonic Nanoparticles 16
2.2.1 Turkevich method 17
2.2.2 Microemulsion method 18
2.2.3 Co-precipitation method 20
2.2.4 Formation of different colors of Ag NPs 21
2.3. Metallic nanoparticles in biomedicine 23
2.4. Ag NPs cytotoxicity 24
3. Goals 27
3.2. Specific goals 28
4. MATERIALS AND METHODS 29
4. 1 Materials 29
4.1.1 Reagents used for the synthesis of Ag NPs 29
4.1.2 Equipments used for the synthesis and characterization of Ag NPs 29
4.1.3 Reagents used the evaluation of colloidal stability of Ag NPs 29
4.1.4 Equipment used to determine the mean hydrodynamic size and zeta potential of Ag NPs 30
4.2 Experimental setups 30
4.2.1. Ag NPs synthesis using a flow reactor 30
4.2.2 Description of single experiments 32
4.2.2 Steric stabilization with non-ionic surfactant 37
4.2.3 In vitro cytotoxicity evaluation 38
5. RESULTS AND DISCUSSION 40
5.1 Synthesis of Ag NPs using a flow reactor 40
5.1.1 Experiment I - performed in a flow reactor at the CAU 40
5.1.2 Experiment II - performed in a flow reactor at University of Kiel 41
5.1.3 Experiment III - performed in a flow reactor at University of Kiel 42
5.1.4 Experiment IV - performed in a flow reactor at the University of Kiel 44
5.1.5 Experiment V - performed in a flow reactor at the University of Kiel 45
5.1.6 Experiment VI - performed in a flow reactor at the University of Kiel 47
5.1.7 Experiment VII - performed in a flow reactor at the University of Kiel 47

5.1.8 Experiment VIII - performed in a flow reactor at the University of Kiel 48
5.2 Synthesis of Ag NPs performed in a batch reactor at the synchrotron light source – Experiment IX.....49
5.2.1 In-situ absorption measurements of Ag NPs synthesis.....50
5.2.2 Synchrotron-based in-situ XRD analysis of Ag NPs synthesis.....51
5.2.3 Ex-situ XRD analysis after Ag NPs synthesis 52
5.2.3 Comparison of simultaneously performed in-situ XRD analysis absorption and pH measurements during Ag NPs synthesis.....53
5.3. Evaluation of colloidal stability of Ag NPs 54
5.3. Cytotoxicity analysis.....57
6. CONCLUSIONS.....60
REFERENCES.....61

1. INTRODUCTION

Metal nanoparticles exhibit optical properties that can be used for different applications ranging from building chemical species sensing devices, photovoltaic devices, to mediating or inducing chemical reactions of molecules on surfaces. The key to any of these applications is the excitation of coherent modes of oscillation of the surface electrons of these nanostructures, known as surface plasmon. Thus, whatever the desired application, understanding the optical or spectroscopic characteristics of nanoparticles that support surface plasmon excitation is critical (GRASSESCHIA et.al.,2020).

Some of the metallic nanoparticles that are best known for having the plasmon resonance characteristics are gold nanoparticles (Au NPs) and silver nanoparticles (Ag NPs). While gold ingot is yellow and silver ingot is gray, the coloration of Ag NPs and Au NPs will depend directly on their shape and size, and can have all the colors of the rainbow, from red, green to violet (KRAJCZEWSKI,J et.al., 2017).

The intense coloration and color variety of Au NPs and Ag NPs is due to the plasmonic excitation on their surface. The metals have a positively charged atomic nucleus surrounded by a plasma with free electrons for conducting bands. The surface plasmon resonance (SPR) is a collective oscillation of the plasma electrons near the surface of the nanoparticles when they are irradiated, as evidenced in Figure 1 (KRAJCZEWSKI,J et.al., 2017).

Figure 1: Schematic of plasmon oscillation in spherical plasmonic nanoparticle showing the displacement of the conduction electron charge cloud relative to the nuclei.

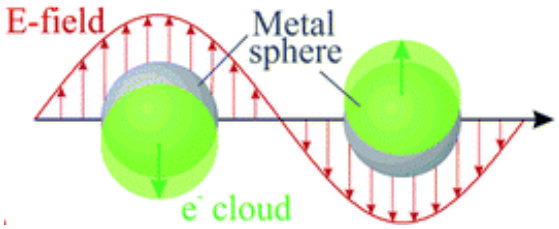

Source: KRAJCZEWSKI,J et.al. (2017)

Due to the specific properties of NPs, they have been used in several areas, as antibacterial agents, in health products, medical device coatings, optical sensors, in cosmetics in the pharmaceutical industry, in diagnostics, as drug delivery systems, as well as anticancer agents (ZHANG et al., 2016). Recently Ag NPs have shown cytotoxic effects on tumor cells. However, it is important to mention that the fundamental characteristics of metallic nanoparticles depend directly on their size, shape, structural configuration, and crystallinity. Therefore, by controlling these parameters upon their synthesis it is possible to obtain the desired properties of these NPs (RAZA et al., 2016).

In the literature are described many methods of syntheses for obtaining plasmonic nanoparticles. The most used is based on the method employed by Turkevich, in which occurs the reduction of Ag or Au from a reducing agent (TURKEVICH; STEVENSON; HILLIER, 1951). In addition, it is important to point out that there are many reports which approach *ex-situ* methodologies, as in ZHANG et al., (2016), where UV-vis spectroscopy, X-ray diffractometry (XRD), Fourier transform infrared spectroscopy (FTIR), X-ray photoelectron spectroscopy (XPS), dynamic light scattering (DLS), scanning electron microscopy (SEM), transmission electron microscopy (TEM), and atomic force microscopy (ATM) analyses were made. However, this type of analysis is not advantageous, considering that during the reaction modifications in particle size and shape can occur and this will directly affect its application (LEDWITH; WHELAN; KELLY, 2007).

The use of flow reactors to synthesize NPs has attracted a lot of attention, since they have several advantages when compared to batch reactors, such as improved heat and mass transfer, phase separation, allowing greater control over the size and shape of these NPs, and greater flexibility in analyzing the mechanisms of each phase (BABER et al., 2015).

It is known that NPs, specifically Ag NPs, have a varied number of applications in the pharmaceutical industry, acting in drug-delivery systems, for example. However, recent studies focus on improving the performance and reducing the cost of these Ag NPs and not on increasing their biological compatibility and in reducing potential risks to human health. Therefore, it is necessary to evaluate the risks of physiological interactions between cells and Ag NPs, as well as the cytotoxicity from these nanomaterials (LI; WANG, 2021).

This work will address the synthesis, characterization, and a preliminary evaluation of Ag NPs cytotoxicity. We propose a synthesis of Ag NPs in a flow reactor, which will allow the realization of *ex-situ* and *in-situ* analysis. After the synthesis of Ag NPs, cytotoxicity tests were performed in RAW 264.7 murine macrophage cell line. The results presented in this work were generated by experiments performed at Christian Albrechts University of Kiel (CAU), Germany, at the German Electron Synchrotron (DESY) and at the Laboratory of Pharmaceutics and Nanotecnology (LDGNano), School of Pharmacy, Federal University of Ouro Preto.

2. LITERATURE REVIEW

2.1 Plasmonic Nanoparticles

Nowadays, studies related to nanoscience on behalf of humanity has grown exponentially. One of the major areas of study is the plasmonic nanoparticles due to their magnetic, electronic, and optical characteristics and properties. The properties of the plasmonic nanoparticles guarantee their application in several areas, such as biomedicine, biotechnology, materials science (solar cells), nanocatalysis and computer science as shown in Figure 2 (THIRUMURUGAN *et.al*., 2011).

Figure 2: Application of metal nanoparticles (MNPs) in various fields.

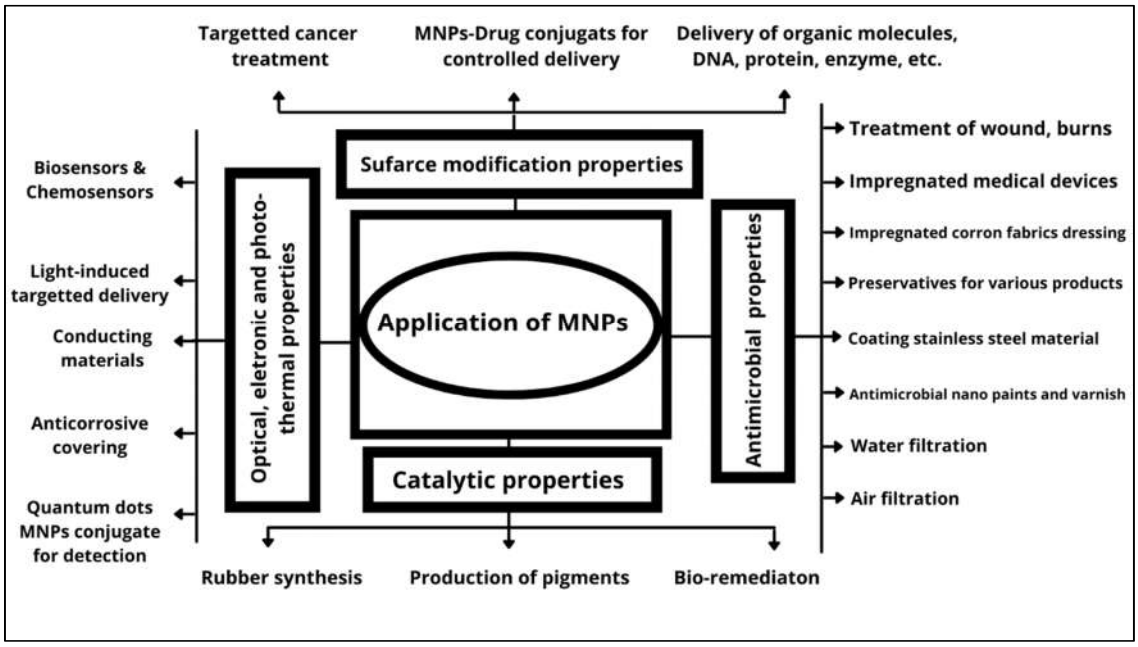

Source: Adapted of THIRUMURUGAN *et al.* (2011)

Although the interest has grown over the past few years, plasmonic nanoparticles have been known by humanity for a long time. The literature describes, for instance, the discovery of a possible gold "solution" in the 4th and 5th century b.c. in China and Egypt. In former times, this "solution" was used for cosmetic and healing purposes, besides for generating a ruby coloration in glass. Years later, it was discovered that this ruby coloration in glass came from the reaction of heterocoagulation of gold

particles with titanium dioxide, which formed colloidal gold as a product. (DANIEL *et. al.,* 2004)

One of the best-known objects related the synthesis of plasmonic nanoparticles is the famous Lycurgus cup (Figure 3), which is on display at the British Museum in London. The constitution of this cup involves thousands of silver and gold nanoparticles. When the cup is struck by light, the electrons belonging to the metals vibrate in a way that changes the color depending on the angle of view of the observer. Historians claim that the addition of the metal nanoparticles to the cup was not an accident or coincidence, since the exact mixture and density of the used plasmonic particles necessary for resulting in these specific optical properties (ARVIZO et al., 2012).

Figure 3: The Lycurgus cup. Gold and silver NPs in the glass resulted in incredible and unique color effects.

Source: ARVISO *et al*. (2012)

Although plasmonic NPs have been present in humanity since a long time, it was in 1857, that Michael Faraday, published the first scientific study on metallic NPs in colloidal systems. Faraday reported that the optical properties of colloidal solutions of gold and silver were dependent on the size of the particles. Then, after a few years and especially nowadays, the use of Ag NPs has drawn a lot of attention and several synthesis methodologies have been tested (ARVIZO *et al.*, 2012).

2.2 Synthesis of Plasmonic Nanoparticles

For the preparation of Ag NPs, there are physical, photochemical, biological and chemical synthetic routes. In each of these routes, there may be benefits and drawbacks, the latter associated with problems intrinsic to the synthesis methodology, either by problems related to degradation, size or shape of Ag NPs, for example (XU et al., 2020).

Chemical methods are widely used for the synthesis of Ag NPs. In these methods, redox reactions are performed, where the values of the standard reduction potentials (E^0) will define the appropriate reagents for the ideal chemical conversion. Hence, for an oxireduction reaction to occur, the Gibbs free energy must be negative, i.e. $\Delta G < 0$, and the standard potential of the redox reaction must be positive, i.e. $\Delta E > 0$. When analyzing the synthesis of silver in aqueous solution, it is known that the standard potential of the reduction of silver in water is considerably high. Thus, it is possible to use various reducing agents. The most used reducing agents include sodium borohydride, hydrazine, and sodium citrate as shown in Table 1 (KRUTYAKOV *et al.,* 2008).

In the literature, several synthesis methods for the preparation of plasmonic nanoparticles are described. In the case of silver nanoparticles, most of them area based on the reduction of silver in a solution of silver nitrate using one or more reducing agents, such as sodium citrate, sodium borohydride, hydrazines, formaldehydes, hydroxylamines, saturated and unsaturated alcohols and sugars (CASANOVA, M.C.R., 2010).

Table 1: Standard potential of silver and examples of commonly used reducing agents in the synthesis of silver nanoparticles.

Reducing agent	**Standard reduction potentials (E^0)**
Silver (Ag)	E^0 = + 0, 799 V
Sodium borohydride ($NaBH_4$)	E^0 = - 0, 481 V
Hydrazine (N_2H_4)	E^0 = - 0, 230 V
Trisodium citrate ($C_6H_5Na_3O_7$)	E^0 = - 0, 180 V

Source: KRUTYAKOV et al. (2008)

For the synthesis of silver nanoparticles using physical methods, the high speed of the process and the avoidance of toxic chemicals are the most important advantages. According to PACIONI *et al.* (2015) the most widely used physical methods for the preparation of metallic nanoparticles are arc discharge and physical vapor deposition.

In addition to chemical and physical methods, silver nanoparticles can be formed from photochemical methods that involve the photoreduction of a precursor or silver ions from a radical, or other intermediate specie, which is photochemically active. Among the benefits of this preparation are the high degree of purity, the procedure is relatively simple, and various reaction media can be used for this synthesis, such as polymers, micelles, emulsions, etc. (GHORBANI *et al.,* 2011).

It is known that conventional methods for nanoparticle synthesis involve silver precursors, reducing agents and, when there is biological interest, the addition of stabilizers/encapsulants is required to prevent Ag NPs from aggregation From this, biological synthesis methods have been developed, consisting of the use of biomolecules as an alternative to reducing/stabilizing agents. Furthermore, it is important to highlight those bacteria, plants and fungi stand out for their activity when it comes to the production of metal nanoparticles (CASTRO, G.R *et al*.,2013).

As evidenced above, there are several alternatives for the synthesis of plasmonic nanoparticles. The most used method for the synthesis of plasmonic NPs is the Turkevich, in which there is the use of a reducing agent that will act in the colloidal solution of gold or silver (TURKEVICH; STEVENSON; HILLIER, 1951), this method will be explained in detail below.

2.2.1 Turkevich method

One of the most used synthesis methods for the synthesis of Ag NPs is the Turkevich method (TURKEVICH; STEVENSON; HILLIER, 1951). It consists in adding sodium citrate ($Na_3C_6H_5O_7$) in a colloidal solution, which contain ions of gold or silver. The sodium citrate will act as the reducing agent and will have the function of reducing the metallic ions of the colloidal solutions to lead to the formation of plasmonic nanoparticles. In addition, the citrate acts as a stabilizer causing an electrostatic repulsion between the NPs. The accepted mechanism for Turkevich involves two

steps, the first being the redox reaction and the second being the deprotonation reaction as shown in Figure 4 (KIMLING *et al*., 2006).

Figure 4: Schematic representation of the protocol of the Turkevich's method applied for the synthesis of plasmonic NPs, using gold as example.

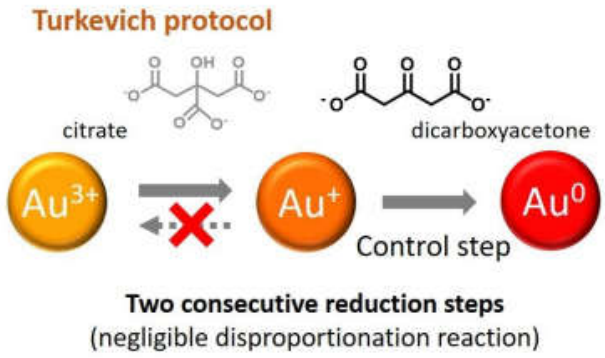

Source: GAO, Y. *et al.* (2020)

Some studies improve the techniques used by the Turkevich approach, as cited in FRENS, G. (1973), where it is evidenced that the concentration of the reducing agent (sodium citrate) interferes directly in the formation of a product. Thus, the concentration of the reducing agent becomes an essential parameter for obtaining plasmonic nanoparticles, since at different concentrations of reducing agents can generates NPs with different properties.

Because the interest in silver nanoparticle has grown greatly over the years, the need to obtain efficient synthesis methodologies has become evident. Several chemical techniques for synthesis of Ag NPs are described in the literature, most associated with the method employed by Turkevich of reduction of colloidal solution. However, the main difference is related to the reagents used in the synthesis and the reaction conditions (LOPES, J.R, 2017).

2.2.2 Microemulsion method

The synthesis of metallic nanoparticles from microemulsion methodologies has been of great interest since the first colloidal solutions of platinum, palladium and

rhodium metal were prepared in the mid-1980s. However, it was only in 1990 that the synthesis of Ag NPs was performed in water-in-oil microemulsions, being quite evident in the literature the importance of obtaining controlled parameters to achieve small-sized and monodisperse particles (SOLANKI; MURTHY, 2011).

Microemulsions are known to be thermodynamically stable and often optically transparent. They are isotropic dispersions of water and liquid hydrocarbons that are stabilized by surfactant molecules. As a structural characteristic, they are ideally monodispersing spherical droplets (diameter <100 nm) of water in oil (w/o) or oil in water (o/w), depending on the nature of the applied surfactant (SOLANKI; MURTHY, 2011).

The water-in-oil type microemulsions act as the reaction medium for the synthesis of nanoparticles, offering a steric barrier by the surfactant, preventing the formation of particulate precipitates, hindering the aggregation of the metallic particles, as evidenced in Figure 5 (SOLANKI; MURTHY, 2011).

Figure 5: Stabilizing silver nanoparticles (Ag NPs) by steric repulsive forces.

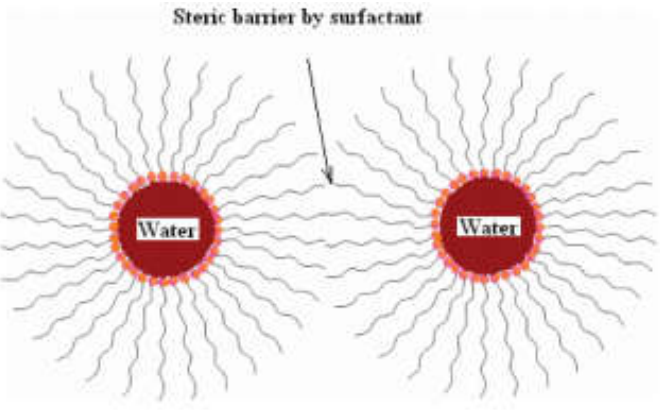

Source: SOLANKI; MURTHY (2011)

Two types of microemulsion methods are described in the literature for the synthesis of nanoparticles. The most widely used, especially for Ag NPs is the double microemulsion method, where a microemulsion containing silver ions is reacted with a solution containing the reducing agent, as evidenced in Figure 6. The collisions and coalescence of droplets result in the formation of a silver precipitate (SOLANKI; MURTHY, 2011).

Figure 6: Schematic representation of the synthesis of SNPs with water-in-oil (w/o) microemulsion

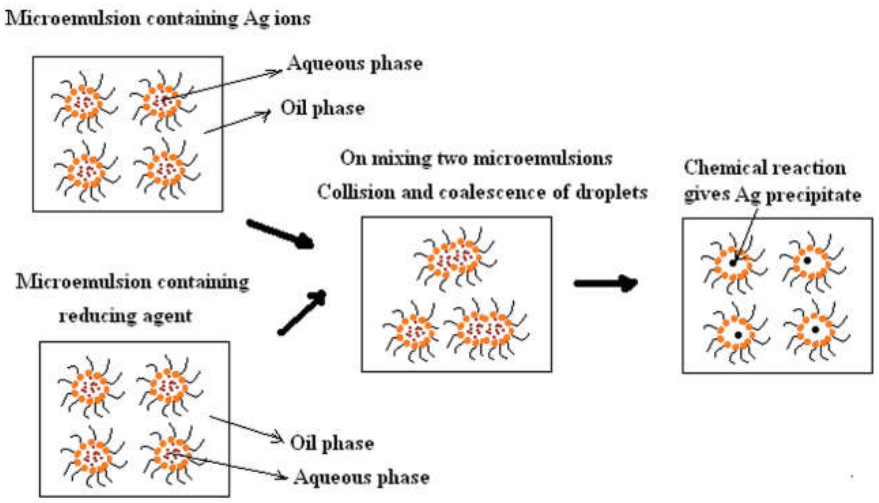

Source: SOLANKI, N.J *et al.* (2011)

As mentioned above, some of the applications of plasmonic nanoparticles depend directly on their shape and size. Therefore, it is important to highlight that the microemulsion method is advantageous due to the possibility of precise controlling of the size of the nanoparticles (SOLANKI, N.J *et al*., 2011).

2.2.3 Co-precipitation method

The co-precipitation method is based on the mixture of anions and cations, forming products with low solubility. When the anion responsible for the formation of the insoluble salt is added, there will be a change in the pH of the solution (aqueous or not), generating the precipitation as a consequence. The nucleation phase will occur simultaneously with the process described above, and several small particles will be produced (KOLTHOFF, I.M.1931).

One of the great advantages of the co-precipitation method is that small-sized nanomaterials can be obtained homogeneously from chemical reactions in solution. The co-precipitation technique is probably the simplest and most convenient chemical technique to synthesize nanoparticles. It is worth noting that the nanoparticles formed

are not stable and can easily aggregate, so many studies have reported alternatives to circumvent this disadvantage, such as the use of a surfactant (LIU, S.S. *et al.,* 2011).

2.2.4 Formation of different colors of Ag NPs

The methodology of synthesis used to obtain silver nanoparticles used in this work was based on the processes described in MENDIS, P. *et.al* (2016), which used the co-precipitation method. Authors reports that the methodology evidenced in the article presents a significant progress in several aspects, because it addresses issues related to the synthesis and stability of nanoparticles of various colors.

In contrast of what had been reported in previous articles, where silver nanoparticles were obtained in non-spherical morphologies, MENDIS, P. *et.al* (2016) obtained most spherical Ag NPs. This is advantageous, since several studies have been reported evaluating the toxicity, stability, and biological compatibility of these spherical nanoparticles, consequently increasing the applicability of the synthetized Ag NPs.

MENDIS, P. *et.al* (2016) highlights an easy and reproducible technique for the preparation of silver nanoparticles of a range of colors. This color variation is mainly due to the size of the spherical nanoparticles. The combination of various sizes of Ag NPs results in different plasmon resonance bands that lead to the production of different colors, and these colors are modified from the concentration of the reactants in the medium.

Figure 7 shows the color spectrum of Ag NPs solutions obtained from different concentrations of reagents and Figure 8 shows an individual absorption spectrum for each of the reactions made by MENDIS, P. *et al.* (2016), where it is possible to observe on the horizontal axis the wavelength and vertical absorption values. As highlighted earlier, the plasmon resonance of the Ag NPs surface, leads to an electron oscillation and it resonates with the magnetic frequency of the electron movement, a strong absorption is observed resulting in the respective colors of the Ag NPs suspensions.

Figure 7: Photograph of (a) Violet (b) Blue (c) Purple (d) Green (e) Yellow (f) Orange and (g) Red Ag NPs suspensions

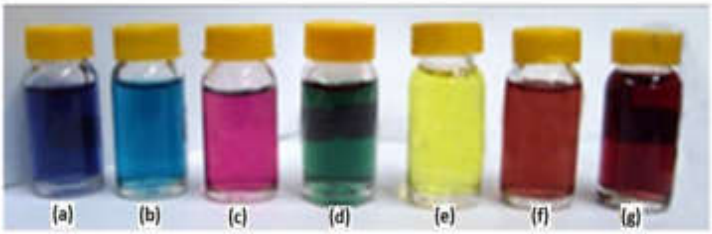

Source: MENDIS, P. *et al.* (2016)

Figure 8: Absorption spectra of different colors of silver nanoparticles suspensions (a) Violet (b) Blue (c) Purple (d) Green (e) Yellow (f) Orange (g) Red.

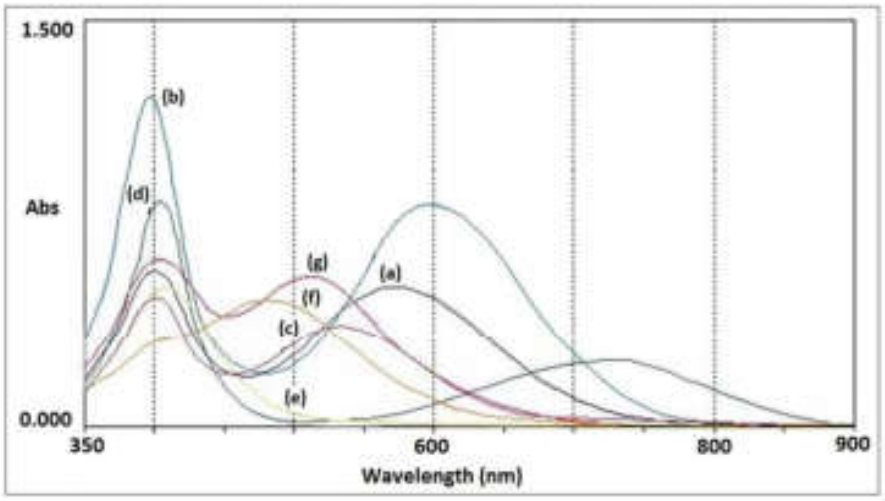

Source: MENDIS, P. *et al.* (2016)

For the synthesis of Ag NPs, MENDIS, P. *et al.* (2016) uses silver nitrate as the precursor solution. As a reducing agent and also as a stabilizing agent sodium borohydrate is used, while as secondary reducing agents hydrazine sulfate and tri sodium citrate are also applied. Sodium citrate has been used as a stabilizing agent as well.

In the experiments conducted by MENDIS, P. *et al.* (2016) it was evidenced that in the synthesis of Ag NPs, the most stable products and able to produce different colors of Ag NPs, are obtained when the reaction process is carried at room

temperature. Furthermore, it was concluded that the best pH to produce Ag NPs in different colors is 10. For avoiding agglomeration and ensuring a high stability under storage, it is advised to store Ag NPs in a refrigerator at a temperature of 4°C.

2.3. Metallic nanoparticles in biomedicine

Nanotechnology is bringing several important aspects related to treatment and diagnostics in the field of biomedicine. The coating of nanoparticles with biologically active substances such as specific ions, antibiotics and analogous substrates or antibodies enables the NPs to cross endothelial barriers and accumulate in target cells without reaching normal cells. Moreover, the physical and chemical characteristics of NPs (size, charge, shape, etc.) play an important role related to biodistribution and cellular internalization of the active agents being carried (COSTA, A. M. *et al,* 2017).

Studies on the possible applications of nanomaterials as carriers for controlled drug delivery, protein and cell separation, bacterial detection and multimodal imaging probes have been increasing over the last years. Due to the variety of possible applications of metallic NPs in biomedicine, the interest in obtaining multifunctional NPs is very high, thus leading to the use of different nanomaterials in order to obtain more than one functionality in a single nanostructured system (MORAES, D.A, 2012).

Among the various applications of NPs in biomedicine, it is evidenced in the literature that Ag NPs are associated with cellular responses, which include antioxidant and cytotoxic actions, due to the formation of reactive oxygen species and the oxidative stress caused by the interaction between the particles and the cell, as shown in Figure 9 (KARLSSON, *et.al.,*2014). Furthermore, due to oxidative stress, Ag NPs can favor anti-inflammatory responses coming from the body (GIOVANNI, M *et al.,* 2015).

Figure 9: Cytotoxic effect of drug conjugated silver nanoparticles.

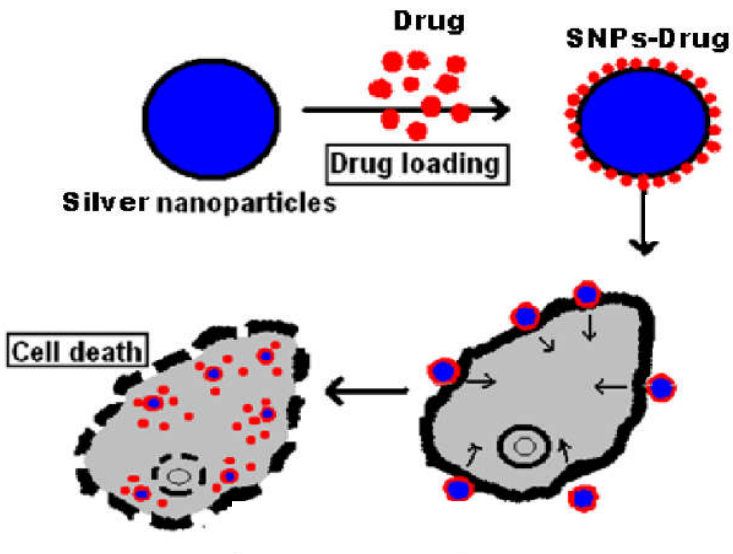

Source: THIRUMURUGAN *et al.* (2011)

2.4. Ag NPs cytotoxicity

In previously published articles it has been reported that the physical and chemical properties of Ag NPs directly affect their toxicity to biological systems. For example, particle size determines the surface area of Ag NPs and may determines how the particles enter the cells (SOUZA, T.A *et al*., 2016). Importantly, although Ag NPs in nanomedicine is well known and extremely important, there is still a gap regarding their toxicity, as few articles indicate the local and systemic toxicity effects of Ag NPs (LIU, X *et.al*., 2021).

The Ag NPs have diverse fields of application in biomedicine, acting as antibacterial agents, drug delivery systems, and physical treatment agents. Several types of toxicity have been detected after exposure to silver nanoparticles, such as changes associated with oxidative stress, cell death by apoptosis, changes in gene expression, and lipid oxidation (SANGOUR, M.H *et. al.,* 2021).

Silver nanoparticles produce distinct toxic effects depending on several factors such as particle size, silver concentration and of the cell type. Results from both mouse and human studies conducted *in vivo* have shown low toxicity. However, it is clear that

there is a need for more investigations with longer exposure times and evaluation in physiological systems that have not yet been studied. The use of reference materials and integrated toxicological studies are of fundamental importance to advance the knowledge and regulation involving Ag NPs (DURÁN, N *et.al.,* 2019).

As it is known, cancer is one of the most complex diseases of humans and is characterized by uncontrolled and widespread growth of abnormal cells caused by various factors. One of the great challenges of humanity today is to find an effective treatment for cancer. Then, due to the antitumor properties of Ag NPs, the interest in these nanomaterials is growing (ZHANG, X *et.al.,* 2016).

In a study conducted by SANGOUR *et al.* (2021) there is evidence that the use of Ag NPs has positive effects on MCF-7 cells (the human breast cancer cell model), decreasing cell viability, will reduced toxicity toward Vero cells, the non-tumoral cell model. SANGOUR *et al.* (2021) concluded that related to the cytotoxicity of Ag NPs, they are selective against tumor cells.

Several studies concerning toxicity analyses of Ag NPs toward a wide range of cell lines are reported in the literature. Different synthetic routes are reported for the preparation of Ag NPs, as well as different concentrations and particle sizes of Ag NPs, as shown in Table 2.

Table 2: Cell line, particle size, concentration and IC50 for Ag NPs reported on literature

Cell Line	Particle Size	Concentration	IC_{50}	References
HepG2	5, 50, and 75 nm	0, 12.5, 25, 50, and 100 µg/mL	100 µg/mL of 5-nm Ag NPs was the most toxic, killing 51% of HepG2 cells	(SUN et al., 2021)
A549	5, 50, and 75 nm	0, 12.5, 25, 50, and 100 µg/mL	100 µg/mL of 5-nm Ag NPs was the most toxic, killing 63% of A549 cells	(SUN et al., 2021)
HaCaT	54.14 – 111.12 nm and 46.89 – 75.23 nm	10 - 1000µg/mL	-	(LI; WANG, 2021)
Macrophages RAW 264.7	54.14 – 111.12 nm and 46.89 – 75.23 nm	10 - 1000µg/mL	-	(LI; WANG, 2021)
MCF-7	-	12.5, 25, and 100 µg/mL	MCF-7 viability was clearly reduced in a dose-dependent manner since the viability decreased to 60% when the concentration was increased to 100 µg/mL	(SANGOUR et al., 2021)
Vero (normal cells)	-	12.5, 25, and 100 µg/mL	Ag NPs exhibited almost no effect on viability of Vero cells at 100 µg/mL Ag	(SANGOUR et al., 2021)

3. Goals

After a deep review in the literature, it was possible to identify that the control of the synthesis of silver nanoparticles is the key for the effectiveness of their applications, from physical to biological applications. At one hand, several synthesis methods and mainly *ex-situ* characterization approaches are reported related to Ag NPs. On the other hand, *ex-situ* characterization techniques do no guarantee a precise and effective control of the synthesis, because they are performed outside the reactor.

The studies of cell viability after exposition to different metallic NPs are widely used. As evidenced in Table 2 of section 2.4, cytotoxicity tests are reported for different types of Ag NPs due the great interest in the use of Ag NPs as tumor biomarkers, sensors and drug carriers, for example. Different cell lines have been used with different ranges of Ag NPs concentrations. However, there is still a gap related to the concentration of Ag NPs that are considered toxic for tumor cell lines and healthy cell lines.

In general, this work aims to investigate the structural evolution of Ag NPs, the co-precipitation synthesis based on the method of MENDIS, P. et.al, 2013. In addition, a flow reactor was used to improve the temporal resolution during monitoring the synthesis reactions. For real time resolution tracking the formulation of Ag NPs, synchrotron based X-ray diffraction analysis will be applied.

The cytotoxicity of Ag NPs was tested in mouse macrophage cells, the RAW 264.7 cell line. Macrophages are first defense of our immune system and are distributed by organs such as liver, spleen, bone marrow and lungs. Macrophages are cells specialized in phagocytosis of particulate xenobiotics, colloidal air particles, bacteria, virus and parasites. They show high phagocytic index and metabolic activity. Thus, they are a good cell model to evaluate exposure to Ag NPs and determine preliminary the concentration range of cell toxicity for furthermore elaborated and specialized toxicity tests.

3.2. Specific goals

- Synthesize Ag NPs from the co-precipitation method, using batch and flow reactors.
- Investigation of the influence of the precursors concentration of the Ag NP formation.
- *In-situ* characterization of the Ag using X-ray diffraction analysis of the German Electron Synchrotron (DESY), besides *in-situ* measurements of UV-Vis absorption spectroscopy and pH value.
- *Ex-situ* characterization of the Ag NPs by X-ray Diffraction (XRD), Dynamic Light Scattering (DLS) and UV-Vis absorption spectroscopy.
- Evaluate the effects of steric stabilization on colloidal stability provides by adsorption of a non-ionic surfactant at Ag NPs surface.
- Evaluate the cell viability of macrophages upon exposure to Ag NPs.

4. MATERIALS AND METHODS

4. 1 Materials

4.1.1 Reagents used for the synthesis of Ag NPs

Chemical reagents	Chemical formula	Purity (%)	Manufacturer
Hydrazine sulphate	$N_2H_6SO_4$	pure	Merck
Silver nitrate	$AgNO_3$	99,5 %	VWR Chemicals
Sodium borohydride	$NaBH_4$	≥98 %	Sigma-Aldrich
Trisodium citrate	$Na_3C_6H_5O_7$	pure	Merck

4.1.2 Equipments used for the synthesis and characterization of Ag NPs

Method	Manufacturer	Description
DLS	Beckman Coulter GmbH	Delsa Nano C Particle Analyser
In-situ UV/Vis	Laser 2000 GmbH	RPS-Mini
Metrohm-System	Metrohm AG	Dosing system, temperature module
XRD	Stadi-p (stoe)	Wavelength detector Cu_α = 1,5456 A

4.1.3 Reagents used the evaluation of colloidal stability of Ag NPs

Chemical reagents	Purity (%)	Manufacturer
Sodium Chloride (NaCl)	-	Sinth – São Paulo

Ultrapure Water	pure	Symplicity 185 Water Purification Equipment-MilliQ
Pluronic® F68	-	Sigma Aldrich

4.1.4 Equipment used to determine the mean hydrodynamic size and zeta potential of Ag NPs

Method	Manufacturer	Description
Zetasizer	Malvern Instrument, UK	Nanoseries Nano-ZS

4.2 Experimental setups

We performed nine experiments for the synthesis of Ag NPs, eight of them were conducted from a flow reactor at the Institute of Inorganic Chemistry at Christian Albrechts University of Kiel and one of these experiments was performed in batch regime and conducted at DESY, Hamburg.

4.2.1. Ag NPs synthesis using a flow reactor

For the synthesis of Ag NPs one of the applied methodologies involves the utilization a flow reactor. An automatic dosing system was used for transporting the silver nitrate and the reducing agent solution to the reactor (Figure.10).

Figure 10: Setup applied for the experiments using the flow reactor. Metrohm dosing system used can be seen on the right side.

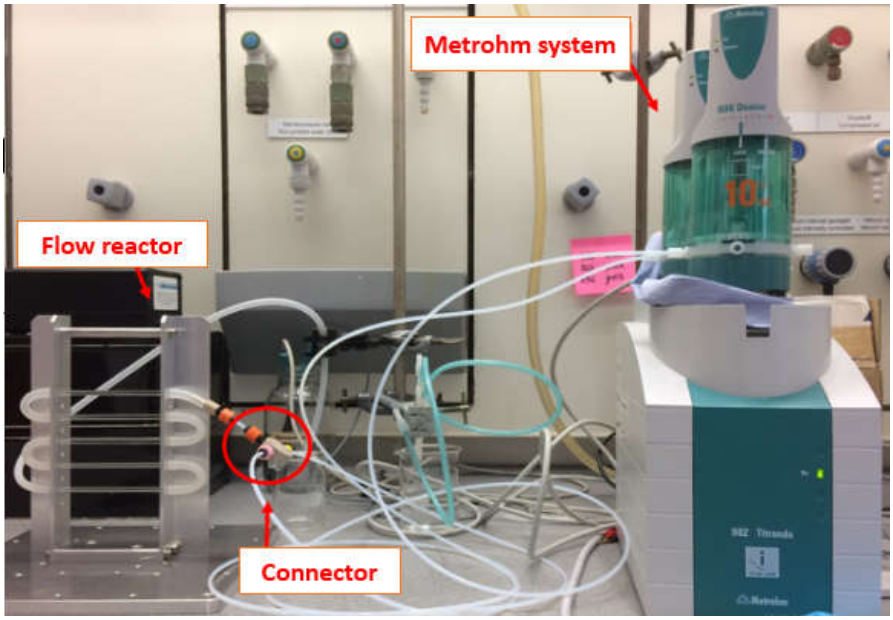

The applied prototype flow reactor features five quartz glass tubes, attached to a metal apparatus, and connected to each other by silicone hoses. The external diameter of the tubes is 4 mm and the internal diameter is 2.5 mm. One of the great advantages of using this reactor is that the tubes are optically transparent in the UV and visible ranges avoiding interferences with the spectroscopic analyses.

4.2.2. Ag NPs synthesis performed in the batch reactor

For performing *in-situ* XRD analyses for monitoring the formation of Ag NPs, the synthesis of Ag NPs was additionally carried out applying a batch reactor at DESY. The high intensity of synchrotron radiation allows the passage of the X-rays through the reactor walls and reaction solution.

For the approach, the silver nitrate solution was prepared and added with aid of dosing system to the reactor containing the reducing agent solution. In addition, this experiment was complemented by *in-situ* measurements of pH value and UV-Vis absorption spectroscopy, as shown in Figure 11.

Figure 11: Setup for experiment conducted in batch regime at the beamline P23 at DESY

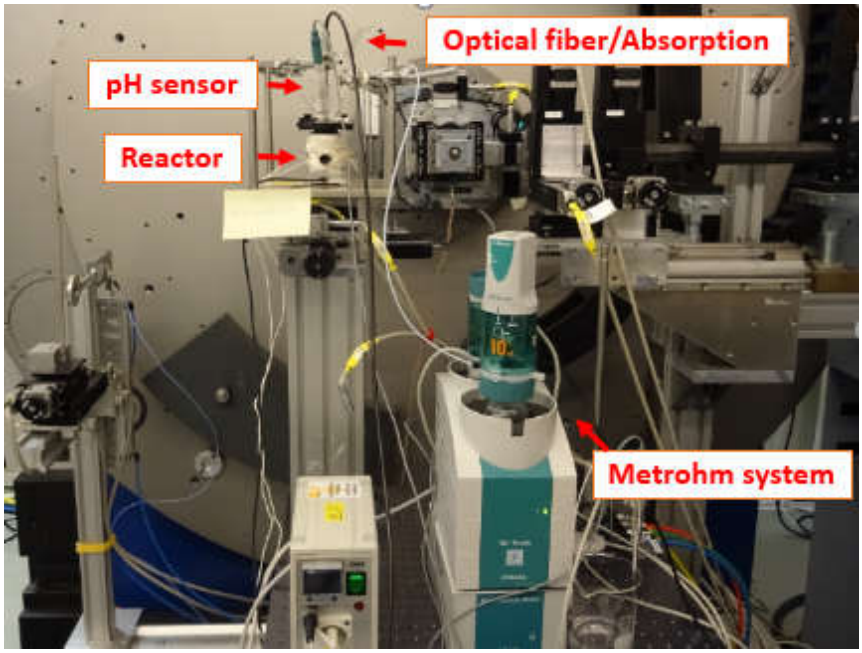

4.2.2 Description of single experiments

For the synthesis of Ag NPs, 9 experiments were conducted, in which different concentrations of the reagents silver nitrate, trisodium citrate, hydrazine sulfate, and sodium borohydride were applied. (Table 3). A variety of reagents concentrations were used to synthesize Ag NPs aiming to evidence different shapes and sizes of the Ag NPs.

Table 3: Concentrations of the reagents used to synthesize Ag NPs in the 9 experiments.

Reactor type	Experiment	Reagents concentrations (mol/L)			
		$AgNO_3$	$Na_3C_6H_5O_7$	$NaBH_4$	$N_2H_6SO_4$
Flow	I	2×10^{-3}	2×10^{-2}	4×10^{-3}	2×10^{-3}
	II	3×10^{-3}	2×10^{-2}	4×10^{-3}	2×10^{-3}
	III	3×10^{-3}	3×10^{-2}	4×10^{-3}	2×10^{-3}
	IV	3×10^{-3}	2×10^{-2}	3×10^{-3}	2×10^{-3}
	V	3×10^{-3}	2×10^{-2}	4×10^{-3}	-
	VI	3×10^{-3}	2×10^{-2}	4×10^{-3}	2×10^{-3}
	VII	3×10^{-3}	3×10^{-2}	4×10^{-3}	2×10^{-3}
	VIII	3×10^{-3}	2×10^{-2}	4×10^{-3}	2×10^{-3}
Batch	IX	1×10^{-2}	1×10^{-1}	3×10^{-2}	2×10^{-2}

4.2.2.1 Experiment I - performed in a flow reactor at CAU

The reducing agents NaBH4 (0.0029g, 0.004 mol/L), $N_2H_6SO_4$ (0.0048g, 0.004 mol/L) and $Na_3C_6H_5O_7$ (0.1546g, 0.02 mol/L) were added to 70 mL of bi-distilled water in container 1 of the dosing system (solution 1). Afterwards, the $AgNO_3$ solution (0.00676g, 0.002 mol/L) was prepared and 20 mL of bi-distilled water was added into container 2 of the dosing system (solution 2).

Programming of the dosing system involved adding 70 mL of the reducing agent solution (solution 1) and 20 mL of the silver nitrate solution (solution 2) to the dosing system, as explained above. After 3 minutes, 3 mL of solution 1 and 3mL of solution 2 were introduced into the flow reactor with a rate of 0.1 mL/min for 30 minutes. After the reaction, product suspension was stirred for 48 hours and centrifuged at a speed of 10,000 rpm for 10 minutes, washed 2 times with 10 mL of water, then washed with 10 mL of ethanol, filtered and placed in the drying oven for 1 hour.

4.2.2.2 Experiment II - performed in a flow reactor at CAU

The reducing agents NaBH4 (0.0036g, 0.004 mol/L), $N_2H_6SO_4$ (0.0051g, 0.002 mol/L) and $Na_3C_6H_5O_7$ (0.1536g, 0.02 mol/L) were added to 70 mL of bi-distilled water in container 1 of the dosing system. Afterwards, the $AgNO_3$ solution (0.0063g, 0.003 mol/L) was prepared and 20 mL of a bi-distilled water was added into container 2 of the dosing system.

Programming of the do system involved adding 70 mL of the reducing agents solution (solution 1) and 20 mL of the silver nitrate solution (solution 2) to the dosing system, as explained above. After 3 minutes, 3 mL of solution 1 and 3mL of solution 2 were introduced into the flow reactor with a rate of 0.1 mL/min for 30 minutes. After the reaction, the product suspension stirred for 48 hours to homogenize the suspension and centrifuged at a speed of 10,000 rpm for 10 minutes, washed 2 times with 10 mL of water, then washed with 10 mL of ethanol, filtered, and placed in the drying oven for 1 hour at t=30 ºC.

4.2.2.3 Experiment III - performed in a flow reactor at CAU

The reducing agents $NaBH_4$ (0.0036g, 0.004 mol/L), $N_2H_6SO_4$ (0.0051g, 0.002 mol/L) and $Na_3C_6H_5O_7$ (0.2327g, 0.03 mol/L) were added to 70 mL of bi-distilled water in container 1 of the dosing system. Afterwards, the $AgNO_3$ solution (0.0062g, 0.003 mol/L) was prepared and 20 mL of a bi-distilled water was added into container 2 of the dosing system.

Programming of the dosing system involved adding 70 mL of the reducing agents solution (solution 1) and 20 mL of the $AgNO_3$ solution (solution 2) to the dosing system, as explained above. After 3 minutes, 3 mL of solution 1 and 3mL of solution 2 were introduced into a flow reactor with a rate of 0.1 mL/min for 30 minutes. After the reaction, the product suspension stirred for 48 hours to homogenize the suspension and centrifuged at a speed of 10,000 rpm for 10 minutes, washed 2 times with 10 mL of water, then washed with 10 mL of ethanol, filtered and placed in the drying oven for 1 hour at t=30ºC.

4.2.2.4 Experiment IV - performed in a flow reactor at CAU

The reducing agents $NaBH_4$ (0.0031g, 0.003 mol/L), $N_2H_6SO_4$ (0.006g, 0.002 mol/L) and $Na_3C_6H_5O_7$ (0.1553g, 0.02 mol/L) were added to 70 mL of bi-distilled water

in container 1 of the dosing system. Afterwards, the $AgNO_3$ solution (0.0036g, 0.003 mol/L) was prepared and 20 mL of a bi-distilled water was added into container 2 of the dosing system.

Programming of the dosing system involved adding 70 mL of the reducing agents solution (solution 1) and 20 mL of the $AgNO_3$ solution (solution 2) to the dosing system, as explained above. After 3 minutes, 3 mL of solution 1 and 3mL of solution 2 were introduced into a flow reactor with a rate of 0.1 mL/min for 30 minutes. After the reaction, the product suspension stirred for 48 hours to homogenize the suspension and centrifuged at a speed of 10,000 rpm for 10 minutes, washed 2 times with 10 mL of water, then washed with 10 mL of ethanol, filtered and placed in the drying oven for 1 hour at t=30ºC.

4.2.2.5 Experiment V - performed in a flow reactor at CAU

The reducing agents $NaBH_4$ (0.0029g, 0.004 mol/L) and $N_2H_6SO_4$ (0.1592g, 0.02 mol/L) were added to 70 mL of bi-distilled water in container 1 of the dosing system. Afterwards, the $AgNO_3$ solution (0.0042g, 0.003 mol/L) was prepared and 20 mL of a bi-distilled water was added into container 2 of the dosing system.

Programming of the dosing system involved adding 70 mL of the reducing agents solution (solution 1) and 20 mL of the $AgNO_3$ solution (solution 2) to the dosing system, as explained above. After 3 minutes, 3 mL of solution 1 and 3mL of solution 2 were introduced into a flow reactor with a rate of 0.1 mL/min for 30 minutes. After the reaction, the product suspension stirred for 48 hours to homogenize the suspension and centrifuged at a speed of 10,000 rpm for 10 minutes, washed 2 times with 10 mL of water, then washed with 10 mL of ethanol, filtered and placed in the drying oven for 1 hour at t=30ºC.

4.2.2.6 Experiment VI - performed in a flow reactor at CAU

The reducing agents $NaBH_4$ (0.0036g, 0.004 mol/L), $N_2H_6SO_4$ (0.0052g, 0.002 mol/L) and $Na_3C_6H_5O_7$ (0.1591g, 0.02 mol/L) were added to 70 mL of bi-distilled water in container 1 of the dosing system. Afterwards, the $AgNO_3$ solution (0.0034g, 0.003 mol/L) was prepared and 20 mL of a bi-distilled water was added into container 2 of the dosing system.

Programming of the dosing system involved adding 70 mL of the reducing agents solution (solution 1) and 20 mL of the silver nitrate solution (solution 2) to the dosing system, as explained above. After 3 minutes, 3 mL of solution 1 and 3mL of solution 2 were introduced into a flow reactor with a rate of 0.1 mL/min for 30 minutes. After the reaction, the product suspension stirred for 48 hours to homogenize the suspension and centrifuged at a speed of 10,000 rpm for 10 minutes, washed 2 times with 10 mL of water, then washed with 10 mL of ethanol, filtered and placed in the drying oven for 1 hour at t=30ºC.

4.2.2.7 Experiment VII - performed in a flow reactor at CAU

The reducing agents $NaBH_4$ (0.0026g, 0.004 mol/L), $N_2H_6SO_4$ (0.0045g, 0.002 mol/L) and $Na_3C_6H_5O_7$ (0.2319g, 0.03 mol/L) were added to 70 mL of bi-distilled water in container 1 of the dosing system. Afterwards, the $AgNO_3$ solution (0.0060g, 0.003 mol/L) was prepared and 20 mL of a bi-distilled water was added into container 2 of the dosing system.

Programming of the dosing system involved adding 70 mL of the reducing agents solution (solution 1) and 20 mL of the silver nitrate solution (solution 2) to the dosing system, as explained above. After 3 minutes, 3 mL of solution 1 and 3mL of solution 2 were introduced into a flow reactor with a rate of 0.1 mL/min for 30 minutes. After the reaction, the product suspension stirred for 48 hours to homogenize the suspension and centrifuged at a speed of 10,000 rpm for 10 minutes, washed 2 times with 10 mL of water, then washed with 10 mL of ethanol, filtered and placed in the drying oven for 1 hour at t=30ºC.

4.2.2.8 Experiment VIII – performed in a flow reactor at CAU

The reducing agents $NaBH_4$ (0.00302g, 0.004 mol/L), $N_2H_6SO_4$ (0.006g, 0.002 mol/L) and $Na_3C_6H_5O_7$ (0.2328g, 0.02 mol/L) were added to 70 mL of bi-distilled water in container 1 of the dosing system. Afterwards, the $AgNO_3$ solution (0.0055g, 0.003 mol/L) was prepared and 20 mL of a bi-distilled water was added into container 2 of the dosing system.

Programming of the dosing system involved adding 70 mL of the reducing agents solution (solution 1) and 20 mL of the silver nitrate solution (solution 2) to the dosing

system, as explained above. After 3 minutes, 3 mL of solution 1 and 3mL of solution 2 were introduced into a flow reactor with a rate of 0.1 mL/min for 30 minutes. After the reaction, the product suspension stirred for 48 hours to homogenize the suspension and centrifuged at a speed of 10,000 rpm for 10 minutes, washed 2 times with 10 mL of water, then washed with 10 mL of ethanol, filtered and placed in the drying oven for 1-hour t=30ºC.

4.2.2.9 Experiment IX – performed in batch at DESY

The reducing agents $NaBH_4$ (0.0569g, 0.003 mol/L), $N_2H_6SO_4$ (0.1319g, 0.02 mol/L) and $Na_3C_6H_5O_7$ (1.290g, 0.1 mol/L) were added to 15 mL of bi-distilled water in container 1 of the dosing system. Afterwards, the $AgNO_3$ solution (0.6792g, 0.01 mol/L) was prepared and 40 mL of a bi-distilled water was added into container 2 of the dosing system.

Programming of the reaction involved adding 15 mL of the reducing agent solution (solution 1) to the dosing system and and 40 mL of the $AgNO_3$ solution (solution 2) in the reactor. After 3 minutes, 5 mL of solution 1 were introduced in the reactor containing the solution 2 with a flow rate of 0.5 mL/min. The reaction time consisted of 60 minutes. After the reaction, the sample stirred for 48 hours to homogenize the suspension and centrifuged at a speed of 10,000 rpm for 10 minutes, washed 2 times with 10 mL of water, then washed with 10 mL of ethanol, filtered and placed in the drying oven for 1-hour t=30ºC.

4.2.2 Steric stabilization with non-ionic surfactant

In each of the 9 samples of Ag NPs, the surfactant Poloxamer 188 was added in an attempt to avoid aggregation of the particles and consequently increase the stability of the Ag NPs in aqueous medium. For this, a solution containing the surfactant Pluronic® F68 was prepared at a concentration of 0.05 mg/mL. Then, nine aliquots of 50 µL of the Pluronic® F68 were pipetted and added into nine Eppendorfs, according to the experiments described on sections 4.2.2.1 and 4.2.2.9. Then 50 µL of each of the nine synthesized Ag NPs suspensions were pipetted and were added into the respective eppendorfs containing the Poloxamer solution, as arranged in the Figure 12.

Figure 12: Schematic representation of the Pluronic® F68 addition in the selected samples from nine experiments of synthesis of Ag NPs.

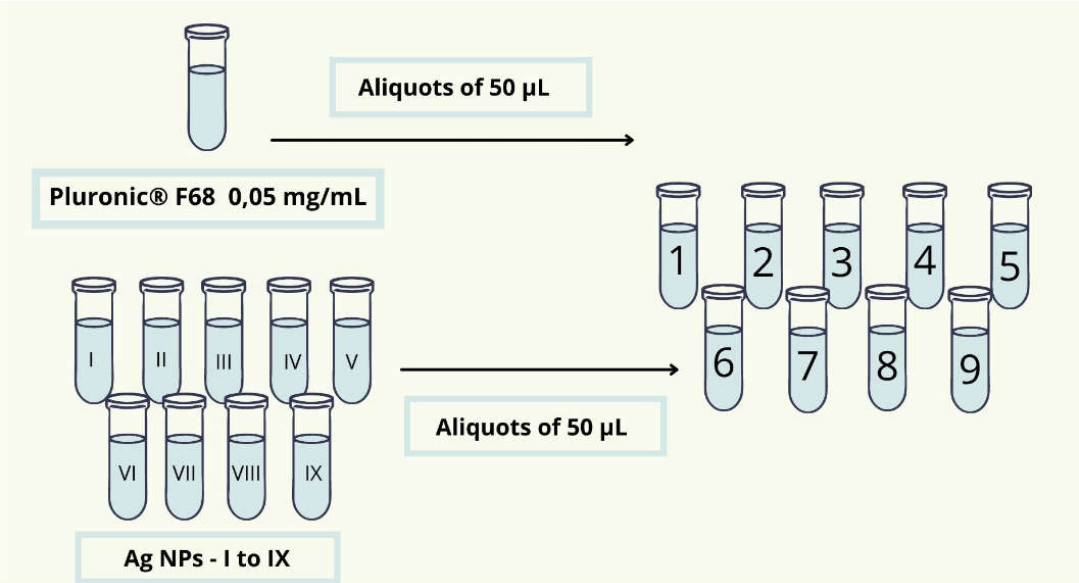

After preparing the samples, particle size distribution (PSD) and zeta potential analyses of the Ag NPs were performed, applying a Zetasizer Nanoseries Nano-ZS (Malvern-UK). The samples were diluted in water, 2 times for size analyses and 1mM NaCl solution (one time) for zeta potential measurements in the respective cuvettes. All analyses were performed in duplicates in each sample. The time-interval between two measurements was 21 days in order to establish the physicochemical stability concerning size dispersion and zeta potential. A comparison between the particle size distribution of the Ag NPs suspensions measured with time difference of 21 days was used for determining the efficiency of the surfactant.

4.2.3 In vitro cytotoxicity evaluation

Cell viability in the presence of different doses of Ag NPs was evaluated *in vitro* with RAW 264.7 murine macrophages cell line. Two samples, experiment II and VIII were selected based on their enhanced homogeneously on size distribution for conducting this experiment. 14 days after suspending the Ag NPs in the Pluronic® F68 solution (section 4.2.2), the samples were washed two times with purified MilliQ water upon centrifugation at 14.000 rpm for 30 minutes to remove residual salts from

synthesis process (Eppendorf 1,5mL, Centrifuges MPW- 260R Med.Instruments). The particles were then dried in oven for 8 hours and the weight of Ag NP was determined and shown in table 4.

Table 4: Quantification of silver present in experiments II and VIII.

Experiment	$m_{initial\ (g)}$	$m_{final\ (g)}$	$m_{Ag\ (g)}$
II	1,21473	1,21478	0,00005
VIII	1,20732	1,20772	0,00040

The cell viability assay was determined under the supervison of Prof. Dr. Vanessa C. F. Mosqueira (Federal University of Ouro Preto) and performed by the PhD student Maria Alice de Oliveira (Federal University of Ouro Preto) by using MTT colorimetric method (Mosssman, 1983). The cell suspensions of RAW 264.7 cells (murine macrophage cell line) (ATTCC TIB-71) were homogeneously distributed in 96-wells microplates at cell density of 1×10^5 cells per well. The plates were incubated for 2 hours at 37 °C and 5% CO_2 for adherence at the bottom of the wells. After the incubation, sample dilutions were prepared in culture medium RPMI 10% SFB with different concentrations (12,5 µg/mL, 25 µg/mL, 50 µg/mL and 100 µg/mL) and incubated for 24 hours at 37 °C and 5% CO_2.

After 24 hours of the addition of the samples, the culture medium was removed and the MTT solution (2 mg/mL in phosphate buffer) was added. After the incubation time, the media was completely removed and DMSO was added to dissolve formazan crystals. Then the microplates were read at 570 nm and the cell multiplication were compared with control without treatment.

5. RESULTS AND DISCUSSION

5.1 Synthesis of Ag NPs using a flow reactor

The experiments I to VIII describe the synthesis of Ag NPs from a flow reactor aiming a future special resolution of the reaction time for improving the temporal resolution of *in-situ* measurements. In summary, the first preliminary experiment I and II were characterized by DLS analyses while for III to VIII, *ex-situ* XRD and DLS analyses were performed. These analyses enabled the identification of the formation of Ag NPs, as well as their particle sizes.

The Ag NPs were obtained, except for experiment V, by mixing the silver nitrate with the solution of sodium borohydride, trisodium citrate and hydrazinium sulphate. The sodium borohydride was mainly responsible for the reduction of the silver salt, the hydrazinium sulphate serves as a supporting reducing agent and the trisodium citrate made a small contribution to the reduction and was mainly used as a capping agent.

5.1.1 Experiment I - performed in a flow reactor at the CAU

During the synthesis of the Ag NPs on experiment I, a strong yellow coloration was observed, especially in the first 2 minutes (Figure 13). It is important to highlight that due to the use of the flow reactor, during the whole reaction time it was possible to visualize the coloration difference with the naked eye. The color change is explained by the evolution of particle size during de Ag NP crystallization, affecting their plasmonic properties. After the end of the synthesis of Ag NPs, the samples were stored under refrigeration.

Figure 13: Experiment I using the flow reactor, enabling visualization with the naked eye of the yellow coloration throughout the reaction (A) and the solution after the synthesis (B)

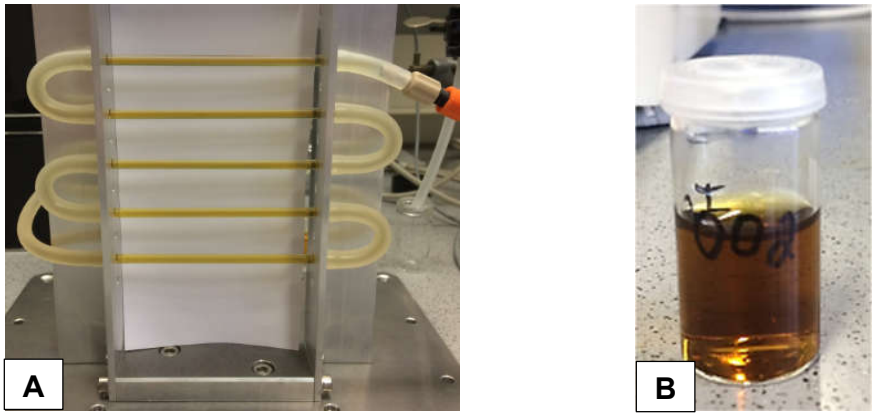

Seven days after the Ag NPs synthesis, the samples were placed in an ultrasonic treatment, in order to destroy large agglomerates and measure the size distribution of the single particles via DLS analyses. The average size of the Ag NPs found is 1.3 ± 0.2 nm.

5.1.2 Experiment II - performed in a flow reactor at University of Kiel

Similar as experiment I, but with different concentrations of precursors, in this synthesis of Ag NPs a strong yellow coloration was observed (Figure 14). After the synthesis the sample was storage at t=4ºC. Seven days after the Ag NPs synthesis, the samples were placed in an ultrasonic treatment, in order to destroy large agglomerates and measure the size distribution of the single particles via DLS analyses. The average size of the Ag NPs found is 1.7 ± 0.3 nm.

Figure 14: Picture of the solution after the synthesis of Ag NPs from the experiment II.

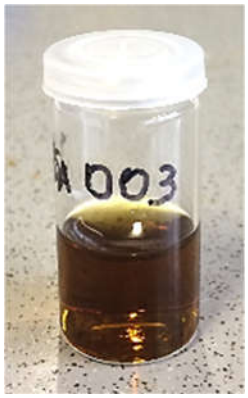

5.1.3 Experiment III - performed in a flow reactor at University of Kiel

In this synthesis of Ag NPs, it was possible to observe the evolution of a rainbow coloration with increasing reactor length and reaction time. Therefore, in the first tube, the Ag NPs suspension was a very light green, then a darker green. In the third tube, a brownish color was observed which then becomes lighter, passing through red and finally an orangey/yellowish color, as shown in Figure 15.

Figure 15: Representation of the flow reactor during experiment III, showing the difference in coloration of the Ag NPs formed during the reaction.

This changes in the color of NPs suspension means that the particles firstly absorb light in the red range of the electromagnetic spectrum, then greenish and blue.

It means an increase on absorption energy for increasing reaction time. However, a redshift of the absorption spectrum is expected for increasing particles sizes of Ag NPs. Exception to this case have been also observed in the literature and attributed to changes in particles morphology according to Mendis *et.al.*

The presence of air bubbles is observed in the reactor, what must be avoided in the future by optimizing the flow rate.

For the experiment III, the sample preparation for DLS analysis were the same used for the previous experiment. The average size of the synthesized nanoparticles was 2.0 ± 0.4 nm. *Ex-situ* XRD analyses were performed for the synthesized silver nanoparticle and compared with the calculated diffraction partners for silver (Figure. 16). The match between measured and calculated diffraction partners confirms the successful synthesis of Ag NPs.

Figure 16: Comparison of the *ex-situ* XRD measurements for experiment III (black curve) with the calculated powder diffraction for silver (red curve).

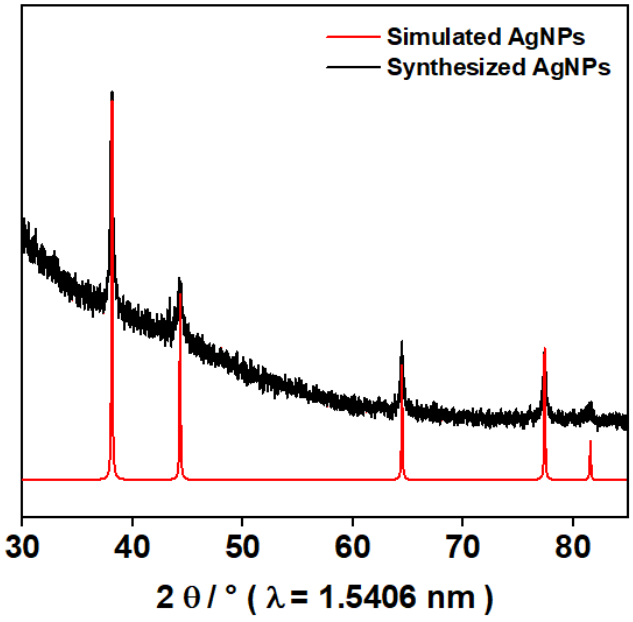

5.1.4 Experiment IV - performed in a flow reactor at the University of Kiel

On experiment IV during the synthesis of the Ag NPs, dark green coloration was observed (Fig. 17). This green color of the NPs suspension indicates the absorbance in the red range of the electromagnetic spectrum. After the synthesis, the sample was storage at t= 4ºC. After seven days, an ultrasonic treatment and DLS analyses were performed. In this case, the average size of the nanoparticles was 2,0 ± 0,4 nm.

Figure 17: Ag NPs suspension after the NPs synthesis on the experiment IV.

As in the experiment III, *ex-situ* XRD analyses were performed. The measured XRD data was compared to the calculated powder diffraction for Ag. In Figure 18, the black curve refers to the measured data of the synthesized sample and the red curve refers to the calculated silver data. A coincidence of the peaks between the measured and simulated data confirms the formation of silver nanoparticles for this experiment.

Figure 18: Comparison of the ex-situ XRD values for product of experiment IV. The black curve represents the measured values and for the red curve the ones for the Ag calculated diffraction partners.

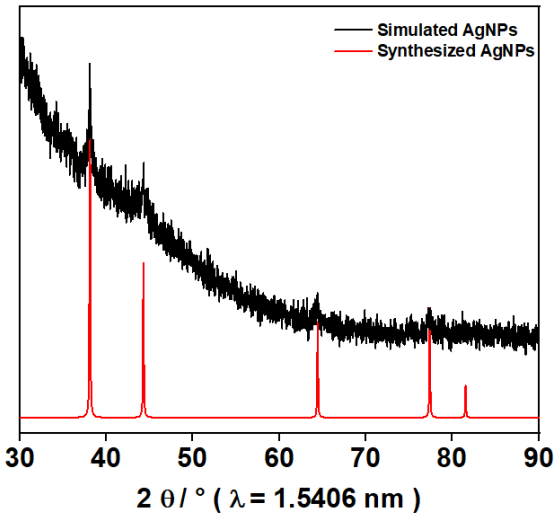

5.1.5 Experiment V - performed in a flow reactor at the University of Kiel

The Ag NPs were obtained from the addition of the silver nitrate solution in the solution containing a solution of sodium borohydride and trisodium citrate. The sodium borohydride was mainly responsible for the reduction of the silver salt, and the trisodium citrate contributed to the reduction and was mainly used as a capping agent.

On experiment V, during the synthesis of the Ag NPs, yellow coloration of the AG suspension was observed (Fig. 19). After the synthesis, the sample was storage at a T= 4 ºC. After seven days, an ultrasonic treatment and then DLS analyses were performed. In this case the average size of the nanoparticles found was 1,3 ± 0,2 nm.

Figure 19: Experiment V using the flow reactor, enabling visualization with the naked eye of the yellow coloration throughout the reaction time.

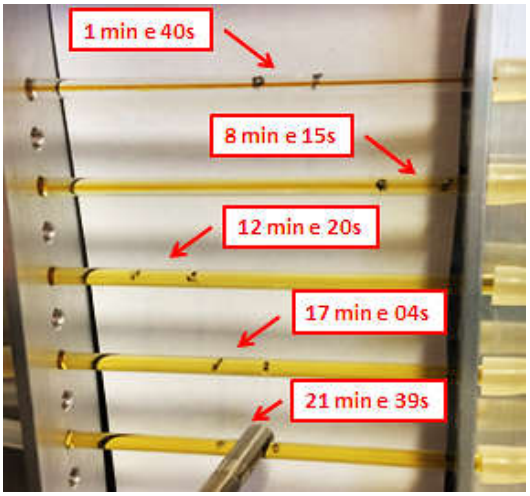

Ex-situ XRD analyses were performed from the powder product after centrifugation. In Figure 20, the red curve represents the data collected from the synthesized sample, while the black refers to the silver calculated.

Figure 20: Comparison of the ex-situ XRD values for product of experiment V. The red curve represents the measured values and for the black curve the ones for the Ag calculated diffraction partners.

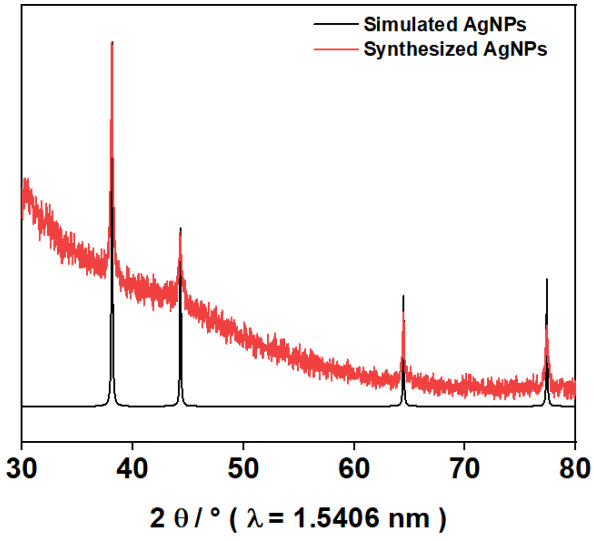

5.1.6 Experiment VI - performed in a flow reactor at the University of Kiel

On this synthesis of Ag NPs, the green coloration of the final suspension was observed (Fig. 21). After the synthesis, the sample was storage at a t= 4ºC. After seven days, an ultrasonic treatment and DLS analyses were performed. In this case, the average size of the nanoparticles was 2,2 $\pm$ 0,5 nm.

Figure 21: The product suspension after the synthesis of Ag NPs from the experiment VI

5.1.7 Experiment VII - performed in a flow reactor at the University of Kiel

In this experiment, a green coloration of the Ag NPs suspension was observed. This color indicates the absorbance of the product in the red spectral range. After the synthesis, the samples treated with an ultrasonic bath for one minute and DLS analyses were performed (Fig.22).

Figure 22: Particle size distribution for product suspension of experiment VII

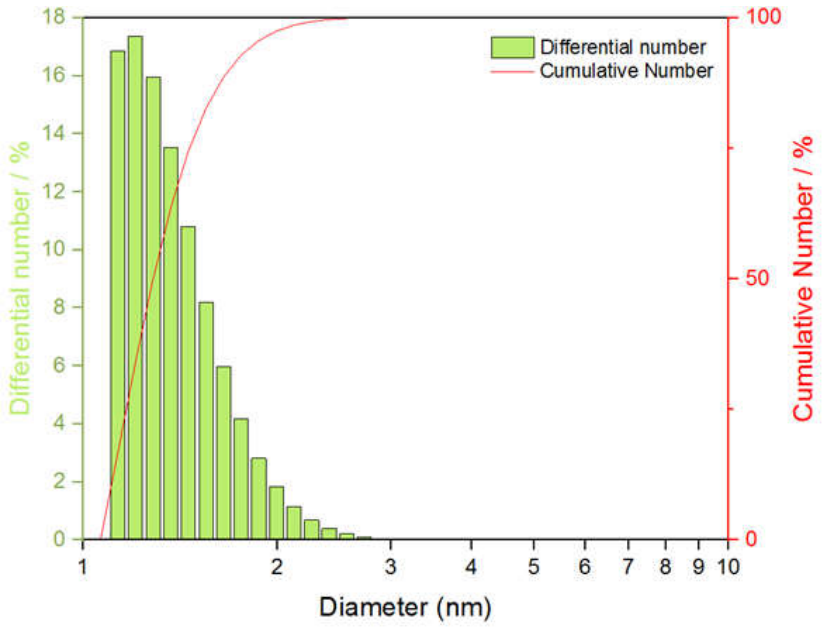

Figure 22 shows the relation of the percentage of differentiation of numbers, the cumulative percentage of numbers and the diameter of the nanoparticles formed. Most of the nanoparticles have diameters between 1 nm and 2 nm, and most of them are smaller than 1.5 nm.

It is also possible to conclude that, although in small quantities, some nanoparticles present a diameter between 2 nm and 3 nm, this experiment results therefore in a very narrow particle size distribution.

5.1.8 Experiment VIII - performed in a flow reactor at the University of Kiel

In this experiment, a red coloration of Ag NPs was observed (Fig. 23). After the synthesis, the samples treated with an ultrasonic bath for one minute and DLS analyses were performed (Fig. 24).

Figure 23: Suspension after the synthesis of Ag NPs from the experiment VIII

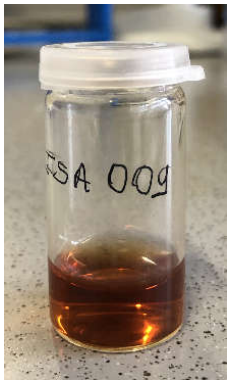

Figure 24: Particle size distribution of product of experiment VIII

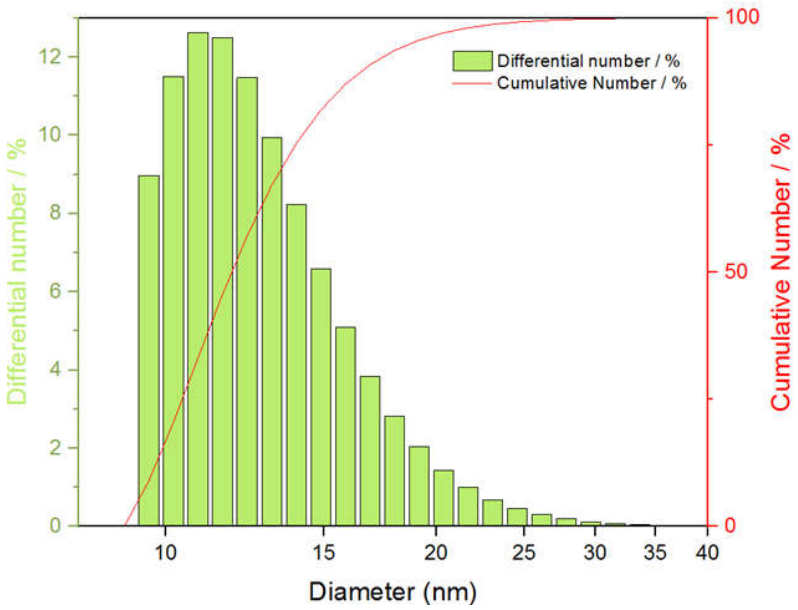

5.2 Synthesis of Ag NPs performed in a batch reactor at the synchrotron light source – Experiment IX

In experiment IX, an increase in the concentration of reagents was necessary for improving the signal-to-noise ratio of the *in-situ* XRD measurements performed at the German Electron Synchrotron, DESY in Hamburg. In addition, the structural evolution of the Ag NPs during synthesis has been monitored by *in-situ* absorbance measurements.

5.2.1 In-situ absorption measurements of Ag NPs synthesis

Figure 25 shows 2D and 3D *in-situ* absorbance measurements recorded during the synthesis of Ag NPs simultaneously to the synchrotron-based *in-situ* XRD analysis. These measurements allow for the better monitoring the changes on optical properties during the Ag NPs formation.

Figure 25: 2D *(A)* and 3D *(B)* plot of absorbance measurements for experiment IX.The experiment was performed on the Beamline P02.1 at DESY, Hamburg.

A) B)

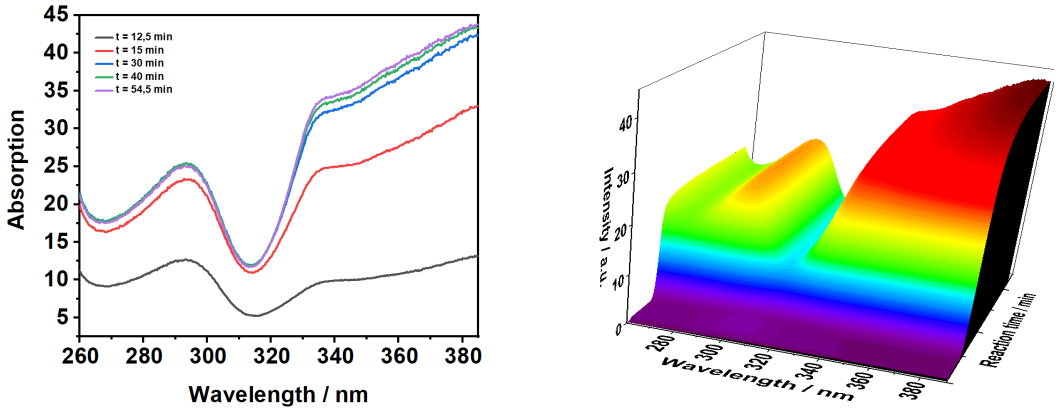

The graphs on Figure 25 represent absorbance measurements versus wavelength as a function of reaction time. This figure shows the recorded spectra between 260 nm and 380 nm, showing their change during the reaction. At approximately 290 nm, the absorption band decreases with time while at 310 nm and at 320 nm absorption bands increase with time.

In detail, the reaction time versus the absorption measurements for different wavelengths is shown in Figure 26. The y-axis (ordinate) shows the normalized absorption, and the x-axis (abscissae) shows the reaction time in minutes. When the reaction time reaches 10 minutes, the addition of the reagents trisodium citrate, borohydrate and hydrazine sulfate to the silver nitrate containing reactor is finished. At approximately 12 minutes there is an increase in the absorbance values, which indicates the formation of the intermediate and then the formation of silver nanoparticles.

Figure 26: Graph of absorbance measurements for experiment IX, comparing reaction time X absorption.

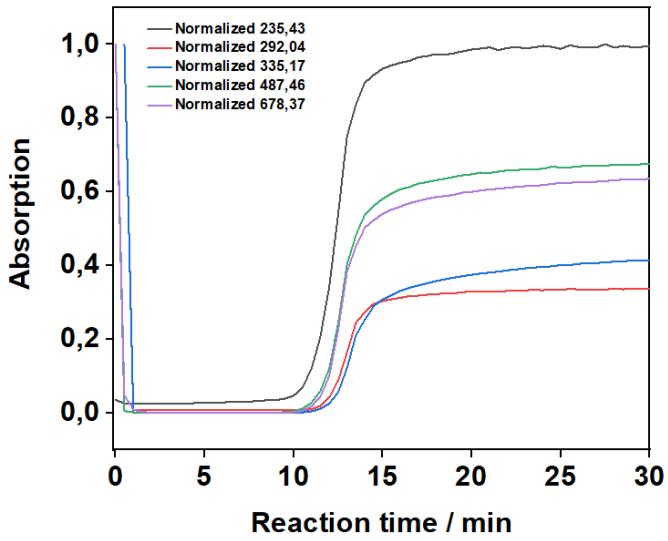

5.2.2 Synchrotron-based in-situ XRD analysis of Ag NPs synthesis

On experiment IX, *in-situ* XRD analysis using synchrotron radiation were conducted intending to confirm the formation of the Ag NPs by monitoring the temporal evolution of the diffraction partners of the synthesized sample and comparing with the calculated values of silver. After this experiment ex-situ XRD analysis was also carried out.

For the *in-situ* XRD analysis (Fig. 27), the red curve represents the calculated XRD values for silver and the black curve represent the *in-situ* XRD data at the determined reaction times during the reaction. The asterisks in the graph marks low-intensity reflexes belonging to a side phase. On the other hand, this diagram shows that the mos intense reflexes belong to the Ag product.

Figure 27: Comparison between the synthesized in-situ X-ray diffraction partners (black curve) and the simulated values for silver (red curve).

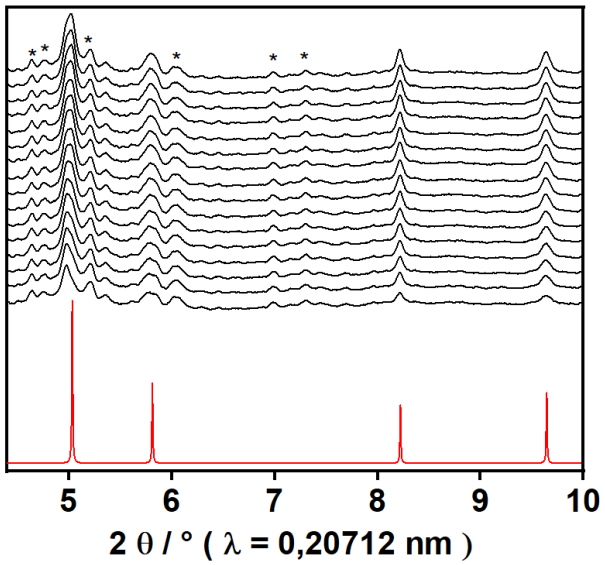

5.2.3 Ex-situ XRD analysis after Ag NPs synthesis

The *ex-situ* X-ray diffraction analysis was performed at the University of Kiel. The measurement was performed at a wavelength of 1.5406 nanometers assigned to the copper radiation of the X-ray diffractometer, which is different from the synchrotron radiation wavelength used for the *in-situ* XRD analysis. In addition, it is important to notice that the *ex-situ* measurements were performed one week after the *in-situ* ones.

Figure 28 shows a comparison of the measured and the calculated diffraction patterns for silver. In this graph, the black curve represents the calculated values, and the red curve represents the result of the XRD analysis. The asterisks as in figure 28 mark the reflexes at a non-identified side phase, similar as observed for the respective *in-situ* measurements. From the analysis of the graph, we conclude that the silver in the sample consists in the main product, since the reflections of highest intensity

Figure 28: Comparison between the ex-situ X-ray diffraction patterns for the synthesized (black curve) and the simulated ones for silver (red curve).

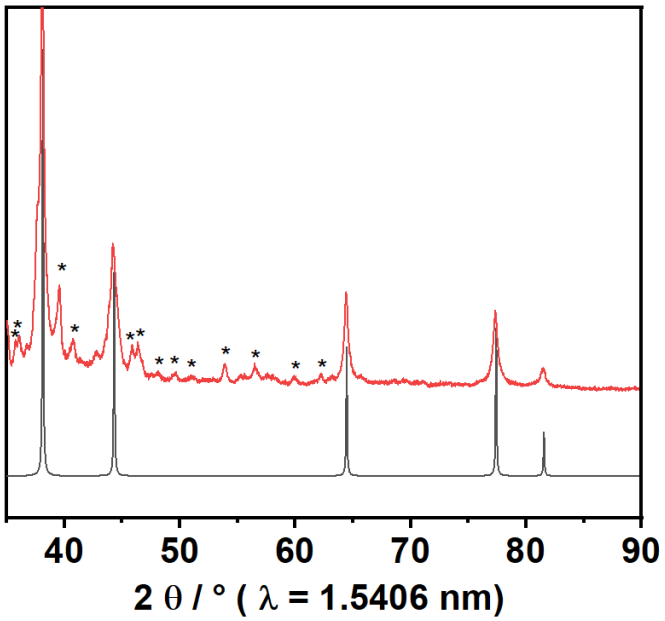

5.2.3 Comparison of simultaneously performed in-situ XRD analysis absorption and pH measurements during Ag NPs synthesis

In summary, 15 mL of the solution of reducing agents was firstly added during 10 minutes to the silver nitrate solution inside the batch reactor (Fig. 29).

During the reaction, the pH value initially oscillated between 6 and 7. At approximately t= 14 min, the pH value decreased to 4,3. The strong variation on pH value indicates a strong change in the reaction solution for example through the product formation. This theory is confirmed by the *in-situ* absorbance and XRD measurement. For example, the X-ray diffraction intensity at 5.01 º2θ assigned to the side phase increases at t=11-14 min together with the reflex at 5,01 º 2θ, assigned to Ag indicating that these two phases are initially simultaneously found.

Figure 29: Comparison between temporal evolution of XRD analysis, absorption and pH measurements during the Ag NPs synthesis.

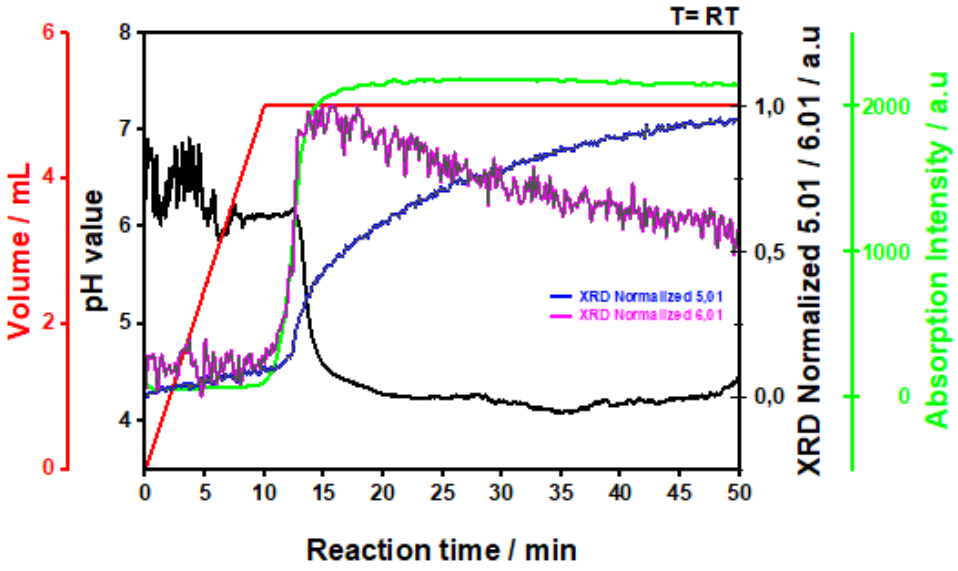

Therefore, it is expected that the side phase is an intermediate, which eventually disappears while the pure Ag product is found. Additional longer experiments are necessary for confirming this hypothesis.

5.3. Evaluation of colloidal stability of Ag NPs

Ag NPs were characterized in terms of size, polydispersity index and zeta potential, and the results were analyzed to verify if the Pluronic® F68 had any influence on these parameters of the Ag NPs synthesized previously. It's important to highlight the fact that the evaluation of colloidal stability was made one year and a half after the Ag NPs synthesis.

The evaluation of the average particle size allows detecting the state of aggregation and sedimentation of the structures as a function of time (REZENDE et al., 2003). Particle size distribution (PSD) analyses were made in duplicate, with 21 days' time-interval between measurements. The table 5 shows the data found in the respective times.

Table 5: Particle size distribution (PSD) values for the Ag NPs synthesized and for the Ag NPs with Poloxamer 188, at T0 (time zero) and at T21 (after 21 days from the first analysis).

	Particle size distribution (PSD) ± SD			
	Ag $NPs_{naked}T_{0\ (nm)}$	**Ag $NPs_{surfactant}T_{0\ (nm)}$**	**Ag $NPs_{naked}T_{21(nm)}$**	**Ag $NPs_{surfactant}T_{21\ (nm)}$**
I	288.20 ± 5.98 (PDI:2.08)	253.80 ± 16.90 (PDI:6.66)	220.70 ± 57.55 (PDI:26.10)	93.50 ± 0.42 (PDI:1,78)
II*	173.2 ± 21.30 (PDI:0.41)	166.40 ± 24.59 (PDI:0.36)	128.20 ± 11.90 (PDI:0.42)	96.90 ± 11.35 (PDI:0.40)
III	774.7 ± 215.8 (PDI:12.30)	798.70 ± 154.10 (PDI:19.30)	547.20 ± 200.30 (PDI:36.60)	739.10 ± 269.50 (PDI:36.50)
IV	461.00 ± 125.40 (PDI:27.20)	434.40 ± 184.70 (PDI:42.50)	287.80 ± 52.00 (PDI:18.10)	345.80 ± 252.60 (PDI:73.00)
V	482.90 ± 17.37 (PDI:3.60)	495.00 ± 153.10 (PDI:30.90)	896.60 ± 458.00 (PDI:51.10)	458.00 ± 33.64 (PDI:13.70)
VI	258.90 ± 45.56 (PDI:17.60)	393.60 ± 141.10 (PDI:35.90)	254.00 ± 6.31 (PDI:26.30)	33.60 ± 3.48 (PDI:16.20)
VII	372.30 ± 39.22 (PDI:10.50)	340.20 ± 20.18 (PDI:5.93)	230.10 ± 1.33 (PDI:37.30)	85.84 ± 2.04 (PDI:23.40)
VIII*	184.80 ± 24.25 (PDI:0.51)	328.00 ± 87.33 (PDI:0.37)	343.10 ± 114.00 (PDI:0.38)	389.00 ± 211.60 (PDI:0.43)
IX	156.80 ± 11.54 (PDI:0.25)	202.00 ± 28.33 (PDI:0.27)	179.70 ± 25.51 (PDI:0.28)	180.00 ± 52.46 (PDI:0.32)

The Ag NPs naked showed sizes in the range of 156.8 to 774.7 nm and 128.2 to 896.6 nm, in the time zero and after 21 days, respectively. For the Ag NPs with Pluronic® F68, the values ranged from 166.4 to 798.7 nm and 33.6 to 739.1 nm, in the time zero and after 21 days, respectively (Table 5).

For the experiments I, II, V, VI and VII, the presence of non-ionic surfactant Pluronic® F68 resulted in a significant reduction in average size after 21 days,

suggesting that over time the interaction between the surfactant and the particles disaggregated the Ag NPs.

Figures 30 and 31 showed the Ag NPs size distribution obtained by experiments II and VIII, respectively. It is possible to observe, in both Ag NPs, the presence of more than one size peak, indicating that the samples present a plurimodal and polydisperse size distribution. This observation is corroborated by the obtained PDI values, which were above 0.3. Furthermore, in both samples, the presence of surfactant did not influence the size distribution.

The evaluation of the zeta potential allows inferences about the physical stability of the developed systems, since it evaluates the electric potential in the shear plane (SOARES et al., 2012). Zeta potential analyses were made in duplicate, with 21 days' time-interval between measurements, and the results are showing in table 6.

Table 6: Zeta potential values for the Ag NPs synthesized and for the Ag NPs with Poloxamer 188, at T0 (time zero) and at T21 (after 21 days from the first analysis).

	Zeta Potential (mV) ± SD			
	Ag $NPs_{naked}T_0$	**Ag $NPs_{surfactant}T_0$**	**Ag $NPs_{naked}T_{21}$**	**Ag $NPs_{surfactant}T_{21}$**
I	-28.00 ± 0.26 mV	-28.10 ± 0.60 mV	-29.90 ± 0.40 mV	-28.00 ± 0.53 mV
II	-42.80 ± 2.03 mV	-36.00* ± 0.81 mV	-39.30 ± 2.10 mV	-41.90 ± 4.70 mV
III	-31.60 ± 0.850 mV	-28.80* ± 3.85 mV	-37.30 ± 4.62 mV	-
IV	-44.60 ± 4.17 mV	**-37.70* ± 1.70 mV**	-46.10 ± 5.88 mV	-44.90 ± 2.18 mV
V	-30.20 ± 3.13 mV	-44.80* ± 4.15 mV	-28.70 ± 6.69 mV	-30.30 ± 9.02 mV
VI	-43.4 0 ± 2.84 mV	**-31.80* ± 1.33 mV**	-27.50 ± 6.31 mV	-33.90 ± 3.48 mV
VII	-42.10 ± 0.306 mV	**-33.50* ± 1.19 mV**	-38.90 ± 1.33 mV	-37.80 ± 2.04 mV
VIII	-41,00 ± 0.15 mV	**-33.80* ± 1.14 mV**	-42.20 ± 6.61 mV	**-35.30 * ± 2.52 mV**
IX	-39.70 ± 1.97 mV	**-27.30* ± 2.67 mV**	-45.70 ± 4.05 mV	**-38.00* ± 2.30 mV**

*Significant reduction of zeta potential values ($p < 0.05$) using unpaired Student *t*-test (confidence interval set at 95%). SD: standard deviation.

The Ag NP display surface charges due to the presence of ions adsorbed at the double electrical layer. In all measurements these charges are negatives. The Ag NPs naked showed potential zeta in the range of -28.0 to -44.6 mV and -27.5 to -46.1 mV, in the time zero and after 21 days, respectively. For the Ag NPs with Pluronic® F68, the values of zeta potential ranged from -27.3 to -44.8 mV and -28.0 to -44.9 mV, in the time zero and after 21 days, respectively (Table 6).

It is known that higher values of zeta potential (in modulus) beneficial factor to increase the colloidal stability of particles, because the electrical repulsion increases (REZENDE et al., 2003). Soares and collaborators (2012) described that a value close to |60| mV is considered an optimal measure of zeta potential for metallic NPs. However, measurements close to |30| mV already guarantee the colloidal stability of nanostructures, maintained better dispersion homogeneity in size and preventing aggregation. The zeta potential values obtained were in general higher than 28 mV for Ag NPs suggesting good physical stability.

Upon adsorption of a non-ionic surfactant, in some samples the amount of the surface charges was significantly reduce (in modulus) as highlighted in bold in Table 6. In one sample the negative value increased (experiment V).

Absorption of non-ionic surfactant, such as Pluronic® F68, reduces the values of zeta in modulus, due to steric effect (GUTERRES et al., 2010; MOSQUEIRA et al., 2000). Thus, it is probable that Pluronic® F68 is able to be adsorbed at Ag NPs surface and increases particle homogeneity of colloidal dispersion reducing “caking effect” and irreversible aggregation.

The negative charge zeta potential and the steric effects provided by PEG chains at NPs surface contribute to the colloidal stability of a system (COUVREUR et al., 2002). These are factors that favor negative potential values zeta: formation of hydrogen bridges between polymeric constituents, dipole-dipole type interaction and the type of surfactant used (SOARES et al., 2012).

5.3. Cytotoxicity analysis

The cell viability of RAW 264.7 murine macrophages cell line exposed to silver nanoparticles obtained by experiments II and VIII was determined using the MTT colorimetric method for 24h incubation. The test was performed using the

concentrations of 12.5; 25.0; 50.0 and 100.0 µg/mL for the JSA008 formulation and the concentrations of 25.0; 50.0 and 100.0 µg/mL for the JSA002 formulation. Cell viability was calculated in comparison with control (untreated) cells.

The cell viability values obtained are shown in Figure 32. For the experiment II, a significant ($p<0.0001$) reduction in cell viability was observed for the concentrations of 50 µg/mL and 100 µg/mL when compared to the control cell. However, a difference in cell viability was not observed between the treatments with the concentrations of 50 µg/mL and 100 µg/mL ($p=0.0786$).

For the experiment VIII, a significant ($p=0.034$) reduction in cell viability was observed only for the 50 µg/mL concentration, when compared to the control cell.

Thus, for the experiment II a dose-dependent profile of cytotoxicity is observed in these macrophages, under our experimental condition. This is consistent with the lower sizes, which in general are phagocytized faster and in a high extent compared with larges NP (sizes).

Significant differences were observed between 25 and 50 µg/mL of JSA 002 Ag NPs where 50 µg/mL induces a 50% inhibition of cell viability. This indicates that IC_{50} is near 50 µg/mL for this cell line with JSA 002 particles.

Figure 30: Cell viability of RAW 264.7 cells after treatment with Ag NPs for 24h

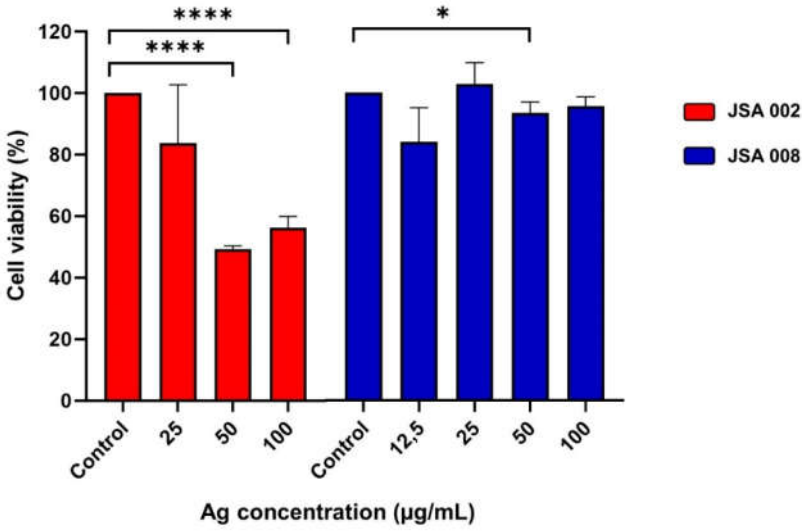

Source: Maria Alice Oliveira[1]

[1] PhD student at the LDG nano laboratory - School of Pharmacy UFOP

Oppositely, the Ag NPs on the experiment VII induces no significant toxicity to these cells, and no dose-dependent effect on macrophages. These differences may be attributed to their differences in size. It is well known that size play a major role in the ability of cell to internalize nano and microparticles and consequently the NPs induces different process of cell death, such as necrosis, apoptosis, and autophagy. More investigations are necessary to unveil the effects of these Ag NPs on cell viability.

6. CONCLUSIONS

Ag NPs were prepared by the co precipitation synthesis using flow and batch reactors. The method used in this work provide a real time resolution during the synthesis of the Ag NPs enabling a precise *in-situ* analysis. This work evidenced that the concentration of the reagents influences directly on the size of the Ag NPs and consequently on their applications by using different concentrations of reagents in the experiments.

Real time resolution permitted to identify the coloration change of the Ag NPs during the synthesis. The reason for the color change is explained by the growing of the particle size during the Ag NPs crystallization and affecting their plasmonic properties. After particle size analysis, it was determined that the yellow Ag NPs presents 1.3 ± 0.2 nm and 1.7 ± 0.3 nm, green Ag NPs presents 2.2 $\pm$ 0.5 nm and orange Ag NPs 2.0 ± 0.4nm.

The synchrotron based XRD in batch reactor evidenced the formation of two phases. One phase the formation of Ag NPs was confirmed and the other phase it's an unknown intermediate evidenced on Fig.28. For the first time *in-situ* analysis were made during the synthesis of the Ag NPs and the use of the flow reactor to synthetize these particles was reportedly here for the first time.

The colloidal stability of the Ag NPs was evaluated from the addition of Pluronic® F68 and it was observed that after the addition of the surfactant the Ag NPs were more homogeneous, i.e. there was a decrease in aggregation. The synthesized Ag NPs are polydisperse.

Evaluation of cytotoxicity allowed the conclusion that cell toxicity of Ag NPs is dependent on the concentration of Ag NPs for sample JSA 002, however is no dose-dependent for experiment VIII. For sample JSA 008, there was no decrease in viability, i.e., Ag NPs were not cytotoxic in toward the RAW 264.7 cells macrophages, whereas for experiment II at higher concentrations, cell viability decreased significantly (~50%), evidencing dose-dependence.

REFERENCES

ARVIZO, Rochelle R. et al. Intrinsic therapeutic applications of noble metal nanoparticles: past, present and future. **Chemical Society Reviews**, v. 41, n. 7, p. 2943, 2012. Disponível em: <http://xlink.rsc.org/?DOI=c2cs15355f>.

BABER, Razwan et al. Synthesis of silver nanoparticles in a microfluidic coaxial flow reactor. **RSC Advances**, v. 5, n. 116, p. 95585–95591, 2015. Disponível em: <http://xlink.rsc.org/?DOI=C5RA17466J>.

CASANOVA, Monise Cristina Ribeiro. Síntese, caracterização e estudo da estabilidade de nanopartículas metálicas estabilizadas com polieletrólitos e tióis. 2010, 87 f. Tese (Mestrado em Ciências- química analítica) – Universidade de São Paulo, São Carlos, 2010;

CAUERHFF, Ana; CASTRO, Guillermo R. Bionanoparticles, a green nanochemistry approach. **Electronic Journal of Biotechnology**, v. 16, n. 3, p. 11-11, 2013.

COSTA, Alessandro Mariano; SILVA, Viviane Viana. Estratégias nanotecnológicas para diagnóstico e tratamento do câncer. **Revista Saúde e Meio Ambiente**, v. 5, n. 2, p. 1-13, 2017.

COUVREUR, P.; BARRATT, G.; FATTAL, E.; VAUTHIER, C. Nanocapsule Technology: A Review. **Critical Reviews in Therapeutic Drug Carrier Systems**, v. 19, n. 2, p. 99–134, 2002.

DANIEL, M.C, Astruc, D. Gold Nanoparticles: Assembly, Supramolecular Chemistry, Quantum-Size-Related Properties, and Applications toward Biology, Catalysis, and Nanotechnology. **Chem. Rev**. 2004, 104, 293−346

DE OLIVEIRA, M. A. et al. IR780-polymer conjugates for stable near-infrared labeling of biodegradable polyester-based nanocarriers. **European Polymer Journal**, v. 120, n. June, p. 109255, 2019.

DURÁN, N *et. al.* Nanotoxicologia de nanopartículas de prata: toxicidade em animais e humanos. **Quim. Nova**, Vol. 42, No. 2, 206-213, 2019

FRENS, Gerrit. Controlled nucleation for the regulation of the particle size in monodisperse gold suspensions. **Nature physical science**, v. 241, n. 105, p. 20-22, 1973.

GAO, Yunhu; TORRENTE-MURCIANO, Laura. Mechanistic insights of the reduction of gold salts in the Turkevich protocol. **Nanoscale**, v. 12, n. 4, p. 2740-2751, 2020.

GHORBANI, H. Reza et al. Biological and non-biological methods for silver nanoparticles synthesis. **Chemical and Biochemical Engineering Quarterly**, v. 25, n. 3, p. 317-326, 2011.

GIOVANNI, Marcella et al. Pro-inflammatory responses of RAW264. 7 macrophages when treated with ultralow concentrations of silver, titanium dioxide, and zinc oxide nanoparticles. **Journal of hazardous materials**, v. 297, p. 146-152, 2015.

GRASSESCHI, Daniel; SANTOS, Diego P. dos. Nanomateriais plasmônicos: parte i. fundamentos da espectroscopia de nanopartículas e sua relação com o efeito sers**.** **Química Nova**, v. 43, p. 1463-1481, 2021.

GUTERRES, S.; POLETTO, F.; COLOMÉ, L.; RAFFIN, R.; POHLMANN, A. Polymeric Nanocapsules for Drug Delivery. In: **Colloids in Drug Delivery**. [s.l: s.n.]. p. 71–98

KARLSSON, Hanna L. et al. Mechanism-based genotoxicity screening of metal oxide nanoparticles using the ToxTracker panel of reporter cell lines. **Particle and fibre toxicology**, v. 11, n. 1, p. 1-14, 2014.

KIMLING, Judith et al. Turkevich method for gold nanoparticle synthesis revisited. **The Journal of Physical Chemistry B**, v. 110, n. 32, p. 15700-15707, 2006.

KOLTHOFF, I. M. Theory of coprecipitation. The formation and properties of crystalline precipitates. **The Journal of Physical Chemistry**, v. 36, n. 3, p. 860-881, 2002.

KRAJCZEWSKI, Jan; KOŁĄTAJ, Karol; KUDELSKI, Andrzej. Plasmonic nanoparticles in chemical analysis. **RSC advances**, v. 7, n. 28, p. 17559-17576, 2017.

KRUTYAKOV, Yu A. et al. Synthesis and properties of silver nanoparticles: advances and prospects. **Russian Chemical Reviews**, v. 77, n. 3, p. 233, 2008.

LEDWITH, Deirdre M.; WHELAN, Aine M.; KELLY, John M. A rapid, straight-forward method for controlling the morphology of stable silver nanoparticles. **Journal of Materials Chemistry**, v. 17, n. 23, p. 2459-2464, 2007.

LI, Yiling; WANG, Wen-Xiong. Uptake, intracellular dissolution, and cytotoxicity of silver nanowires in cell models. **Chemosphere**, v. 281, p. 130762, 2021.Disponível em: <https://linkinghub.elsevier.com/retrieve/pii/S0045653521012339>.

LIU, Xiongwei et al. Nanotoxic effects of silver nanoparticles on normal HEK-293 cells in comparison to cancerous HeLa cell line. **International Journal of Nanomedicine**, v. 16, p. 753, 2021.

LIU, Si Si et al. Enhanced removal of trace Cr (VI) ions from aqueous solution by titanium oxide–Ag composite adsorbents. **Journal of hazardous materials**, v. 190, n. 1-3, p. 723-728, 2011.

LOPES, Josias Rogério. Síntese de nanopartículas de prata (NPSAg) em soluções aquosas de fibroína de seda e gelatina. 2017, 115 f. Tese (Mestrado em Engenharia Mecânica) – Universidade Estadual de Campinas, Campinas, 2017.

MENDIS, Pramujitha et al. Nanosilver rainbow: a rapid and facile method to tune different colours of nanosilver through the controlled synthesis of stable spherical silver nanoparticles. **RSC advances**, v. 6, n. 54, p. 48792-48799, 2016.

MORAES, Daniel Angeli. Nanopartículas magnéticas decoradas com nanopartículas metálicas visando aplicações em biomedicina, 2012, 70 f. Tese (Mestrado em ciências – físico-química) - Universidade de São Paulo, São Carlos, 2012.

MOSQUEIRA, V. C. F.; LEGRAND, P.; PINTO-ALPHANDARY, H.; PUISIEUX, F.; BARRATT, G. Poly(D,L-Lactide) Nanocapsules Prepared by a Solvent Displacement Process: Influence of the Composition on Physicochemical and Structural Properties. **Journal of Pharmaceutical Sciences**, v. 89, n. 5, p. 614–626, maio 2000.

PACIONI, Natalia L. et al. Synthetic routes for the preparation of silver nanoparticles. In: **Silver nanoparticle applications**. Springer, Cham, 2015. p. 13-46.

RAZA, Muhammad Akram et al. Size-and shape-dependent antibacterial studies of silver nanoparticles synthesized by wet chemical routes. **Nanomaterials**, v. 6, n. 4, p.

74, 2016.

REZENDE, S. et al. Caracterização e estabilidade físico-química de sistemas poliméricos nanoparticulados para administração de fármacos. **Química Nova**, v. 26, n. 5, p. 726–737, 2003.

SANGOUR, M.H., Ali, I.M., Atwan, Z.W. et al. Effect of Ag nanoparticles on viability of MCF-7 and Vero cell lines and gene expression of apoptotic genes. **Egypt J Med Hum Genet** 22, 9, 2021.

SOARES, G. et al. Desenvolvimento e caracterização de nanopartículas lipídicas destinadas à aplicação tópica de dapsona. **Química Nova**, v. 35, n. 7, p. 1388–1394, 2012.

SOLANKI, Jignasa N.; MURTHY, Zagabathuni Venkata Panchakshari. Controlled size silver nanoparticles synthesis with water-in-oil microemulsion method: a topical review. **Industrial & engineering chemistry research**, v. 50, n. 22, p. 12311-12323, 2011.

SOUZA, Tiago AJ et al. Cytotoxicity and genotoxicity of silver nanoparticles of different sizes in CHO-K1 and CHO-XRS5 cell lines. **Mutation Research/Genetic Toxicology and Environmental Mutagenesis**, v. 795, p. 70-83, 2016.

SUN, Jiaojiao et al. Silver nanoparticles: Correlating particle size and ionic Ag release with cytotoxicity, genotoxicity, and inflammatory responses in human cell lines. **Toxicology and Industrial Health**, v. 37, n. 4, p. 198–209, 24 abr. 2021. Disponível em: <http://journals.sagepub.com/doi/10.1177/0748233721996561>.

THIRUMURUGAN, G.; DHANARAJU, M. D. Silver nanoparticles: real antibacterial bullets. In: **Antimicrobial Agents**. IntechOpen, 2012. Available from: https://www.intechopen.com/books/antimicrobial-agents/silver-nanoparticles-real-antibacterial-bullet

TURKEVICH, John; STEVENSON, Peter Cooper; HILLIER, James. A study of the nucleation and growth processes in the synthesis of colloidal gold. **Discussions of the Faraday Society**, v. 11, n. c, p. 55–75, 1951.

XU, Li et al. Silver nanoparticles: Synthesis, medical applications and biosafety. **Theranostics**, v. 10, n. 20, p. 8996–9031, 2020. Disponível em: <https://www.thno.org/v10p8996.htm>.

ZHANG, Xi-Feng et al. Silver Nanoparticles: Synthesis, Characterization, Properties, Applications, and Therapeutic Approaches. **International Journal of Molecular Sciences**, v. 17, n. 9, p. 1534, 13 set. 2016. Disponível em: <http://www.mdpi.com/1422-0067/17/9/1534>.